# Stony Brook University

OFFICIAL COPY

# Genetic and structural analyses of poliovirus protein 2C$^{\text{ATPase}}$

A Dissertation Presented

by

**Emmanuel Noble Asare**

to

The Graduate School

in Partial Fulfillment of the

Requirements

for the Degree of

**Doctor of Philosophy**

in

**Genetics**

Stony Brook University

**August 2015**

**Stony Brook University**

The Graduate School

**Emmanuel Noble Asare**


We, the dissertation committee for the above candidate for the

Doctor of Philosophy degree,

hereby recommend acceptance of this dissertation.


**Eckard Wimmer, Ph.D., - Dissertation Advisor**

**Distinguished Professor, Department of Molecular Genetics and Microbiology**


**Carol Carter, Ph.D., - Chairperson of Defense**

**Professor, Department of Molecular Genetics and Microbiology**


**Patrick Hearing, Ph.D.**

**Professor, Department of Molecular Genetics and Microbiology**


**Laurie Krug, Ph.D.**

**Assistant Professor, Department of Molecular Genetics and Microbiology**


**Elizabeth Reider, Ph.D**

**Senior Research Scientist, Foreign Animal Disease Research Unit, USDA, ARS**

**Plum Island Animal Disease Center**


This dissertation is accepted by the Graduate School


Charles Taber

Dean of the Graduate School


ii

**ABSTRACT OF THE DISSERTATION**

**Genetic and Structural analysis oof poliovirus protein 2C$^{\text{ATPase}}$**

by

**Emmanuel Noble Asare**

**Doctor of Philosophy**

in

**Genetics**

Stony Brook University

**2015**

The specificity of encapsidation of members of the genus *Enterovirus* of the *Picornaviridae* family depends on an interaction between capsid proteins and nonstructural protein 2C$^{\text{ATPase}}$. In particular, in the context of a chimeric virus, the $N_{252}$ residue of poliovirus (PV) 2C$^{\text{ATPase}}$ interacts with VP3 E180 of coxsackievirus A20. PV 2C$^{\text{ATPase}}$ has important roles both in RNA replication and encapsidation, but in the context of just the poliovirus polyprotein, $N_{252}$ does not function in assembly. The aim of my study was to search for additional residues near $N_{252}$ in 2C$^{\text{ATPase}}$ that are required for PV encapsidation. I predicted a three-dimensional protein structure of PV 2C$^{\text{ATPase}}$ to assist in the selection of residues used for mutagenesis. Accordingly, segments adjacent to $N_{252}$ were genetically analyzed by combining triple and single alanine mutations to identify individual residues required for function. From four triple alanine mutants, two exhibited defects in RNA replication. The remaining two mutations, located in secondary structures in a predicted three-dimensional model of 2C$^{\text{ATPase}}$, caused lethal growth phenotypes. Most single alanine mutants, derived from the lethal triple variants, were

either quasi-infectious and yielded variants with wildtype (wt) or *ts* growth phenotypes or had a lethal growth phenotype due to a defect in RNA replication. However, a virus harboring a $K_{259}A$ mutation, mapping to an alpha helix in the predicted protein structure of $2C^{ATPase}$ near $N_{252}$, replicated with wt kinetics at $37^oC$, but resulted in a cold-sensitive virus at $33^oC$. *In vivo* protein synthesis and virus production were strikingly delayed at $33^oC$ relative to the *wt* suggesting a defect in uncoating. Studies with a reporter virus indicated that this mutant is also defective in encapsidation at $33^OC$. Cell imaging confirmed a much-reduced production of $K_{259}A$ mature virus at $33^oC$ relative to the wt. In conclusion, we have identified a new residue in PV $2C^{ATPase}$ ($K_{259}A$) that is involved in particle assembly. In addition, we have linked a cold sensitive encapsidation defect mapping to $2C^{ATPase}$ ($K_{259}A$) to a subsequent delay in uncoating of the virus particle during the next cycle of infection at $33^oC$.

# TABLE OF CONTENTS

## LIST OF TABLES

## LIST OF FIGURES

## LIST OF ABBREVIATIONS

BCS             Bovine calf serum

*c.s.*          Cold sensitive

CAV             Coxsackie virus

CD-155          Cellular receptor 155

*Cre*           cis- replicating RNA elements

CPE             cytophathic effect

DAPI            4',6-diamidino-2-phenylindole

DMEM            Dulbecco's modified Eagle medium

EMCV            Encephalomyocarditis virus

FMDV            Foot-and-mouth disease virus

HAV             Hepatitis A virus

HBSS            Hank's buffered saline solution

HRV             Human rhinovirus

hnRNP           Heterogeneous nuclear ribonucleoprotein C

m.o.i.          Multiplicity of infection

PABP            Poly(A) binding protein

PBS             Phosphate-buffer saline

PCBPs           Poly(c) binding protein 2

Phyre2          Protein Homology/analogy Recognition Engine V 2.0 (Phyre2)

PV              Poliovirus

*t.s.*          Temperature sensitive

WHO             World Health Organization

# ACKNOWLEDGEMENTS

**INTRODUCTION**

Poliomyelitis is a frightening infectious disease, caused by poliovirus (PV). PV has led to several epidemic infections during the 20$^{th}$ century. The main characteristic of poliomyelitis is flaccid paralysis caused by the destruction of motor neurons in the central nervous system. The natural hosts of PV are humans and monkeys. PV belongs to the *Picornaviridae* family in the *Enterovirus* genus (FIGURE 1). Picornaviruses are wide-spread in nature, and include many well known viruses like hepatitis A virus (HAV), coxsackie viruses (CAV, CVB), human rhinoviruses (HRV), and foot and mouth disease virus (FMDV). It has been estimated that viruses from this family cause over 4 billion infections yearly. PV is the most studied *Enterovirus* and serves as the best model for the lifecycle of viruses in the genus (discussed below).

I. Early History of Poliovirus

Poliomyelitis dates as far back as the Egyptian 18$^{th}$ Dynasty (1580-1350 B.C.), where relics show the crippled leg of a young man at an Astarte Temple. There are no reports of epidemics of poliomyelitis before Stockholm, Sweden (1889), which suggests that the disease probably occurred in sporadic outbreaks before that time. Historical trends suggest that the transition from sporadic to epidemic forms of poliomyelitis was due to the improvement of sanitary and hygienic conditions. In the 20$^{th}$ Century, during World War I (1916), the United States faced a poliomyelitis epidemic that affected over twenty-seven thousand and fatally killed over six thousand people in New York City alone (Melnick, 1996). Furthermore, a famous and well-liked public figure, Franklin D. Roosevelt, contracted the disease after another poliomyelitis epidemic in 1921, which provided a national incentive to combat the disease. This epidemic initiated a public

interest in the research into poliomyelitis, primarily through the National Foundation for Infantile Paralysis. However, the majority of efforts to fight poliomyelitis were directed toward prevention. Sponsored programs ranged from physical therapy that revitalizes muscles to chemical therapeutics such as antibiotics. Through these failures, a consensus on the development of vaccines eventually became the favorable method for defeating poliomyelitis.  The Noble prize discovery of the rapid isolation of poliovirus in cells by Enders, Weller and Robbins in 1949 (Ender et al., 1949) spurred the formulation of an inactivated vaccine, which was achieved by Salk's group in 1954 (Salk et al., 1954). This was quickly followed by the development of attenuated viruses by Sabin's group in 1955, for the propagation of live attenuated vaccines (Sabin and Boulger, 1973).

II. Present challenges to eradication efforts

Symptoms of poliomyelitis includes aseptic meningitis and persisting weakening of one or more muscle groups; in the skeletal or cranial, which accounts for about 1% of PV infections (Melnick, 1996). Some minor illnesses of PV infections are characterized by malaise, fever, nausea, and sore throat. The majority of infections are asymptomatic (Melnick, 1996). During the coarse of epidemic PV infections, the signs of poliomyelitis generated public disruption and panic, which generated enormous fear of the virus worldwide. The most effective tools to fight poliomyelitis came via the developments of the inactivated polio vaccine (IPV) and live attenuated vaccine (OPV) (Wimmer et al., 1993). The IPV vaccines have to be injected by trained health workers (Salk, 1960; Wimmer et al., 1993). The OPV, on the other hand, is administered by mouth. OPVs also induce local mucous immunity that prevents wild type (wt) PV causation of poliomyelitis

and also spreads to unimmunized people and increases the impact of OPV across the general population (Sabin and Boulger, 1973; Wimmer et al., 1993).

In 1988, the World Health Organization (WHO) launched a global eradication campaign against PV. The eradication campaign has been very successful in reducing global incidents of poliomyelitis. However, there are some setbacks in the eradication campaign, and the WHO's end date has been pushed back twice. Some of the issues affecting the eradication program include conflicts in different parts of the world, such as Pakistan, Afghanistan, Nigeria and others (Pallansch and Sandhu, 2006). In addition, there are few mutations in Sabin's OPV vaccines and the vaccines have genetic instabilities and can accumulate point mutations (Guillot et al., 1994; Kew et al., 2005; Stanway et al., 1984). Lastly, high genetic recombination between poliovirus and other C-cluster enteroviruses generate circulating vaccine-derived polioviruses (cVDPVs) (Arita et al., 2005; Minor, 2009). cVDPVs are particular problems for the overall eradication campaign because they can be as neurovirulent as wt PV (Arita et al., 2005; Jiang et al., 2007). cVDPVs of all three serotypes have been involved in outbreaks of poliomyelitis in various parts of the world that use the OPV vaccinations, such as Hispaniola (Kew et al., 2002), Phillipines (Shimizu et al., 2004), Madagascar ((Rousset et al., 2003), China (Kew et al., 2005), Cambodia (Arita et al., 2005). Though the WHO's vaccination effort was successful in the reduction of signs of poliomyelitis, the actual eradication of PV and of its recombinant variants remains a challenge (Pallansch and Sandhu, 2006).

III. Physical and chemical nature of poliovirus

The success in large cultivation of poliovirus in tissue culture enabled the work on the molecular biological studies of the virus. This eventually led to the isolation of the virus, and also to the determination that the viral RNA was the infectious agent in tissue culture (Alexander et al., 1958). The viral life cycle including protein synthesis, RNA synthesis, encapsidation and release of mature viruses were also studied and described (Darnell, 1958; Levy, 1961). X-ray crystallographic studies and electron microscopic analyses of poliovirus-infected cells were performed in the late 1950s (Finch and Klug, 1959; Horne and Nagington, 1959). Moreover, a genetic map of the poliovirus viral RNA was constructed in the late 60's and mid 70's. Translation of the polyprotein from the viral RNA in vitro was described (Kitamura et al., 1981a; Racaniello and Baltimore, 1981; Toyoda et al., 1987), and the linkage of viral protein VPg to the 5'-terminal UMP of the RNA genome was discovered (Rothberg et al., 1978). VPg is the only non-capsid protein that is packaged with the RNA genome.

IV. Poliovirus Genome Organization

The PV genome consists of a small positive strand RNA of about 7500 nucleotides (nt), which contains a 774 nt long 5' non-translating region (NTR) and a short 3'NTR with a poly(A) tail, which flanks an open reading frame (ORF) that encodes a large polyprotein (FIGURE 2). The polyprotein, consisting of 2209 amino acids, is eventually cleaved to produce capsid and replication proteins, including the virus's own RNA polymerase (FIGURE 2) (Kitamura et al., 1981b).

The 5'end of the 5' NTR contains an RNA structural element known as the cloverleaf that is implicated in the formation of replication complexes for both negative and positive RNA synthesis, and is also implicated in the switch from translation to

replication (Andino et al., 1990; Rivera et al., 1988). Downstream of the cloverleaf is another important RNA element called the internal ribosomal entry site (IRES), which promotes the initiation of translation in a cap-independent way (Jang et al., 1988; Pelletier et al., 1988). The RNA of PV does not utilize a m7G cap structure, which is essential for the translation initiation of host cell's mRNAs (Nomoto et al., 1976). PV inhibits host cell protein synthesis via its nonstructural protein 2A[pro] that cleaves translation initiation factors eIF4G, a component of the cap recognizing complex eIF4F that drives cap-dependent translation (Borman et al., 1997; Kräusslich et al., 1987). Since the virus disrupts the host cell's translation machinery, the 5' NTR is critical for viral translation, replication, and overall proliferation of PV.

PV's ORF is translated into one large polyprotein, 247 kDa in size, which is processed into two main domains: structural and non-structural (Kitamura et al., 1981a; Phillips and Fennell, 1973; Summers and Maizel, 1968). The structural domain (also known as P1), interacts with chaperone heat-shock protein 90 (Hsp90), and is subsequently proteolytically processed by viral protein 3CD[pro] to viral capsid proteins VP0, VP3, and VP1 (Geller et al., 2007). Structural proteins VP0, VP3, and VP1 immediately form a 5S protomer that complexes with four additional protomers to form a 14S pentamer (Hellen et al., 1989; Korant, 1973; Verlinden et al., 2000). Twelve pentamers either assemble to for an empty capsid or condense around the newly made viral RNA to form a noninfectious provirion (Guttman and Baltimore, 1977; Jiang et al., 2014). Provirions eventually undergo a maturation cleavage (VP0 → VP2 and VP4) to form infectious virus particles (Basavappa et al., 1994; Harber et al., 1991; Hellen and Wimmer, 1992; Hindiyeh et al., 1999; Hogle, 2002). Recent evidence shows that the

specificity of encapsidation of the viral RNA is dependent on an interaction of viral

capsid proteins with nonstructural proteins (Liu et al., 2010).

The non-structural region of the polyprotein is divided into P2 and P3 domains

and contains proteins that perform different functions in viral RNA replication and

proliferation (Wimmer et al., 1993). The P2 domain encodes viral proteins $2A^{pro}$,

precursor 2BC, mature proteins 2B, and $2C^{ATPase}$ (Hanecak et al., 1982; Hellen et al.,

1989).  The P3 domain encodes precursor proteins 3AB, 3BC, $3CD^{pro}$, which are further

cleaved into 3A, 3B (VPg), $3C^{pro}$ and $3D^{pol}$ (Toyoda et al., 1986). $2A^{pro}$ is the proteinase

responsible for the first polyprotein cleavage, which is between the structural (P1) and

non-structural region (P2 and P3) at a tyrosine^glycine (Y^G) dipeptide (Korant, 1973).

Subsequent processing of the structural and non-structural domains occur at

glutamine^glycine (Q^G) dipeptides by $3C^{pro}$ and $3CD^{pro}$ (Ypma-Wong et al., 1988).

Encoded at the C-terminus of the P3 region is viral protein $3D^{pol}$, which is an RNA

dependent RNA polymerase.

Due to PV's compact genome size, the viral proteins have multiple and

overlapping functions, such that both precursor and mature proteins have unique

functions (Wimmer et al., 1993). This is advantageous for the virus because it allows for

rapid replication of its viral genome and uses less energy in the production of proteins

(because of the multi-functionality of proteins and unique activity of precursor proteins).

V. Life cycle of poliovirus

The life cycle of the virus will be discussed starting at the time when it has

encountered a host cell with a proper receptor. Prior to this period, the virus is completely

6

inactive and will remain infectious unless the it is destroyed by environmental factors, such as ultraviolet light, heat, bleach, etc.

The life cycle of PV can be summarized in six steps.

a. Receptor binding

The virus enters the cell via host cellular surface receptor CD-155, and is absorbed into the host cytoplasm (Hogle, 2002; Smyth and Martin, 2002; Zhang et al., 2008). Absorption includes a series of events, which dramatically changes the conformation of the capsid caused by the virus-receptor interaction. This leads to the internalization of the infectious virion into the cytoplasm of the host cell by a clathrin and caveolin-independent mechanism (Brandenburg et al., 2007). The uncoating process follows immediately after endocytosis of the virus.

b. Uncoating of the virus and release of the viral RNA

Early studies suggested that the viral RNA was released at the perinuclear region, close to the ribosomes, to stimulate translation of the viral RNA. However, recent evidence suggests that viral RNA release takes place in vesicles close to the cell surface (Brandenburg et al., 2007; Hogle, 2002). Studies in the sequential dissociation of virus *in vivo* are lacking, however, we know that the delivery of the viral RNA is essential for replication. After internalization, the virus forms an A-particle (135S), which has a slower sedimentation coefficient due to the expanded state of the virion (Kohn, 1979; Lonberg-Holm et al., 1975; Maizel et al., 1967). A-particles are described as "leaky" because of an increase in permeability to stains that are not observed for mature viruses. *In vitro* studies suggest that the leakiness of the virion is primarily due to the loss of

7

capsid protein VP4, which destabilizes the capsid and allows the incorporation of small molecules (Katagiri et al., 1967). Interestingly, leaky A-particles still protect the viral RNA from RNase degradation, which indicates that the dissociation of VP4 alone does not lead to the release of the viral RNA. Past *in vitro* uncoating studies suggests that the additional release of VP2 is required before the release of the viral RNA (Curry et al., 1996; Maizel et al., 1967). However, heat degradation experiments suggest that the viral RNAs are released from the capsid shell before the release of VP2 (Jordan and Mayor, 1974). A recent model from the Hogle lab suggest that PV forms a pore-complex on internalized membranes that allows the release of RNA into the cytoplasm (Hogle, 2002). It can be concluded from these studies that the uncoating of PV is a multistep process that requires the release of capsid protein/s (VP4/VP2) before the release of infectious viral RNA into the host cell cytoplasm.

c. Translation of the viral RNA and cleavage of the polyprotein

After the release of viral RNA into the host cell cytoplasm, viral protein VPg is cleaved off from the 5' end and it is translated into a polyprotein (Nomoto et al., 1977). As described above, the polyprotein is cleaved by viral protease $2A^{pro}$ at a Y^G dipeptide and this is followed by subsequent cleavage to precursor and mature proteins by $3C^{pro}/3CD^{pro}$ at Q^G dipeptides (Lawson and Semler, 1992) (FIGURE 2). An additional unknown proteolytic event on capsid protein VP0 generates proteins VP4 and VP2, (VP0→VP4+VP2; maturation cleavage), which is the last step in the generation of the infectious virus particles (Basavappa et al., 1994).


d. Viral RNA Replication

8

The replication of the infectious viral RNA is one of the most important and also a well-studied stage of the viral life cycle. Replication takes place on membranous vesicles of the host cytoplasm (Aldabe and Carrasco, 1995a; Bienz et al., 1987; Cho et al., 1994; De Sena and Mandel, 1977; Doedens and Kirkegaard, 1995; Echeverri et al., 1998; Richards et al., 2014; Teterina et al., 1997). Replication of the viral RNA is performed by the virus's RNA-dependent RNA polymerase protein 3D$^{pol}$, in conjunction with other viral and cellular host factors (Paul and Wimmer, 2015). Replication takes place on membranous vesicle structures that are induced by viral proteins (Bienz et al., 1994). This is where *cis*-acting RNA elements, viral proteins, and cellular host proteins function in a synchronized fashion (Paul and Wimmer, 2015). PV viral proteins 2C$^{ATPase}$, 2BC, and 3A are responsible for the induction of replication vesicles in the host cells (Adams et al., 2009; Aldabe and Carrasco, 1995b; Doedens and Kirkegaard, 1995; Fenwick and Wall, 1973; Teterina et al., 1997). Recent studies have also shown preferential recruitment and enrichment of phosphatidylinositol-4-Phosphate (PIP4) lipids to the membranous structures (Hsu et al., 2010). The compositions of membranous structures have not yet been identified, but they have been shown to contain proteins from both the endoplasmic reticulum and Golgi (Belov et al., 2007; Schlegel et al., 1996). The overall replication occurs in the following steps; plus strands RNA—> minus strand RNA —> replication form (RF) —> replicative intermediate (RI) —> plus strand RNA (Paul and Wimmer, 2015).

RNA intermediates are defined as the RF and RI. The RF consists of a double stranded RNA structure and has higher specific infectivity than single stranded RNA (Bishop and G. Koch, 1967). Whether the RF is a true intermediate in the replication

cycle or just a byproduct of hybridization of the positive and negative viral RNA during purification is not yet known(Detjen et al., 1978; Kuhn and Wimmer, 1987; Paul and Wimmer, 2015). The following intermediate RI, is composed of full-length negative strand RNA and 6-8 nascent positive RNA strands (Baltimore, 1968; Bishop et al., 1969). Due to the partial resistance of the RI to ribonuclease digestion, it is believed that RI contains both single- and double- stranded RNA (Kuhn and Wimmer, 1987; Wimmer et al., 1993). Proteins in the non-structural P2 and P3 domains are particularly important for producing an environment that is conducive for RNA replication, as well as the essential viral proteins for replication. Initiation of the plus strand RNA requires viral and cellular host factors, as well as viral RNA structures, which are further described below.

*RNA structures involved in RNA replication.*

The 5' terminal UMP of the viral RNA is covalently linked to a hydroxyl group of a tyrosine in VPg (3B) (Rothberg et al., 1978). The 5'NTR has a cloverleaf RNA structure, as mentioned above, which is involved in RNA replication and was discovered in 1990 (Andino et al., 1990). The cloverleaf interacts with viral proteins 3CD$^{pro}$ and 3AB, and cellular proteins (PCBP1/2) in a complex to initiate minus strand RNA synthesis (Blyn et al., 1996; Gamarnik and Andino, 2000; 1998; Harris et al., 1994). The 3'NTR RNA structure also interacts with viral proteins 3AB and 3CD$^{pro}$ (Harris et al., 1994). Removal or shortening of the poly(A) results in the reduction in infectivity (Spector and Baltimore, 1974). There is a third RNA structure that is very important for RNA replications called a *cis*-acting replication element (*cre*), which is located in the coding region of 2C$^{ATPase}$ (Goodfellow et al., 2000). The PV *cre* is about 26-29 nucleotides long and contains a 14-nucleotide loop. The location of *cre* is not fixed, it can be moved to several regions of the

genome, including the 5'NTR (Goodfellow et al., 2000; Yin et al., 2003). Biochemical and genetic experiments have demonstrated that the *cre* serves as the template for the uridylylation of VPg (3B) in generating the primer (VPgpU) during RNA synthesis (Paul et al., 2003; 2000; Rieder et al., 2000). Recent studies using synthetic polioviruses identified two additional redundant RNA structural elements in the 3D$^{pol}$ coding region that serve an unidentified role in replication (Song et al., 2012).

*Viral and cellular proteins involved in replication.*

The viral enzyme that plays the main role in viral RNA synthesis, for both negative and positive strands, is the RNA dependent polymerase 3D$^{pol}$, which is the last encoded viral protein (Flanegan and Baltimore, 1977). 3D$^{pol}$ catalyzes the synthesis of VPgpU, the primer for the synthesis of both positive- and minus-strand RNA (Paul et al., 2003). This reaction is stimulated by proteinase 3CD$^{pro}$, which lacks RNA polymerase activity. In addition to proteins of the P3 domain, viral protein 2C$^{ATPase}$ that maps to the P2 region also plays an essential role in viral replication (2C$^{ATPase}$ protein is further described below).

*Cellular proteins involved in viral replication.*

Cellular factors involved in replication includes cellular protein Poly(rC) binding protein 2 (PCBP2), which is an RNA binding protein that interacts with the PV IRES and cloverleaf (Toyoda et al., 2007; Zell et al., 2008). PCBP2 interacts with the PV IRES to enhance translation of viral proteins, and its interaction with the cloverleaf is important for negative strand RNA synthesis (Bedard and Semler, 2004; Gamarnik and Andino, 1998; Toyoda et al., 2007). Viral proteinase 3C$^{pro}$ cleaves PCBP2 during PV infection, which is believed to mediate the switch from viral translation to RNA replication (Perera

et al., 2007). Another cellular protein involved in replication is the heterogeneous nuclear ribonucleoprotein C (hnRNP C), which consists of three C1 and one C2 isoform (Brunner et al., 2010; 2005; Roehl and Semler, 1995). hnRNP C is believed to stabilize the interaction between the 5' and 3' ends of the viral genome, which facilitates the initiation of positive strand RNA synthesis from the negative strand (Paul and Wimmer, 2015). Studies have shown that depletion of hnRNP C in cells results in the reduction of positive strand RNA synthesis and progeny virus production (Ertel at al 2010). In addition to its interaction with the NTR, hnRNP C also interacts with 3CD$^{pro}$, and the non-structural precursors P2 and P3 (Brunner et al., 2010). Host cellular protein poly(A) binding protein (PABP) is also involved in viral replication. PABP interacts with the poly(A) tail of the viral RNA (Herold and Andino, 2001) and with 3CD$^{pro}$. It is suggested that PABP protein interaction with viral RNA is required for circularization of the viral RNA and the initiation of negative strand RNA synthesis.

e. Capsid assembly and encapsidation

The assembly of the protein capsid and proper encapsidation of the viral RNA are the last steps in the viral life cycle. This stage is one of the least understood stages in the infectious cycle. These processes are difficult to study because they are closely linked to the translation of the viral genome and RNA replication. Inhibition of either translation or replication also disrupts viral morphogenesis, since they precede assembly and encapsidation.

The formation of viral particles begins shortly after the translation of the polyprotein. The capsid precursor P1, a 97 kDa protein, is separated from the non-structural (P2 and P3) domains by the viral proteinase 2A$^{pro}$ at a Y/G site (Toyoda et al

1986, Jiang et al., 2014). P1 is rapidly myristoylated at the N-terminal glycine, which tethers the protein to cellular membranes (Chow and Moscufo, 1995; Paul et al., 1987). Cellular chaperone heat shock protein 90 (Hsp90) interacts with P1 and enables its cleavage by 3CD$^{pro}$ at Q/G sites. P1 processing leads to the assembly of the structural proteins VP0, VP3 and VP1yielding a protomer (Teterina et al., 2001). It should be noted that the cleaved capsid proteins stay in a complex at all times. Five protomers assemble to form a 14S pentamer (VP0, VP3, VP1)$_5$ capsid intermediate (Jiang et al., 2014). Twelve of the pentamers condense to produce a 75S empty capsid (Jiang et al., 2014).

Since empty capsids were observed in sucrose gradient experiments, it was initially proposed that the viral RNA was packaged into empty, already formed capsids. However, current studies suggest a model in which the pentamers condense around the viral RNA. Several lines of evidence support this model. First, the 14S pentamers have an affinity for viral RNA *in vitro* and undergo a conformational change after binding to RNA (Nugent and Kirkegaard, 1995), while the empty capsids do not. In addition, the 14S particles interact with newly synthesized RNA to form mature virus during *in vitro* cell-free synthesis of mature PV (Verlinden et al., 2000). Moreover, 14S particles accumulate in the cell during temperature block assays, and rapidly form mature viruses after the block is removed (Rombaut et al., 1990). Also, 14S particles are associated with RNA replication complexes in infected cells and can be crosslinked to viral RNA (Pfister et al., 1995). Furthermore, studies with BSO, an inhibitor of glutathione (GSH) biosynthesis, also suggest that 14S pentamers are critical for the generation of mature viruses, and that the empty capsids are nonfunctional intermediate in morphogenesis (Ma et al., 2014).

Morphogenesis of viral RNA is highly specific, in that only one VPg-linked RNA is encapsidated into virions. Studies with chimeric viruses indicated that the NTRs of the RNA genome do not have any major role in this process and do not contain any packaging signals. (Barclay et al., 1998; Gromeier et al., 1996; Rieder et al., 2003; Wimmer et al., 1993, Jiang et al., 2014).

*A protein-protein mechanism for encapsidation.*

Recovered cVDPVs are recombination products of Sabin vaccines (OPV) and the closely related C-cluster CAVs (FIGURE 3) (Kew et al., 2005) . Our lab has studied in vitro the properties of chimeric viruses where domains of the P1 (structural domain) and non-structural domain P2 were interchanged (FIGURE 4) (Jiang et al., 2007). A chimeric virus where the P1 domain of PV was exchanged with CAV A20 revealed a direct interaction between capsid protein VP3 and PV non-structural protein $2C^{ATPase}$ of CAV20. Direct interactions between the non-structural $2C^{ATPase}$ and the capsid proteins have been further demonstrated through an alanine scanning mutagenesis of charged amino acids in PV $2C^{ATPase}$ protein (Liu et al., 2010). In addition, past studies have shown that $2C^{ATPase}$ directly interact with 14S particles (Rombaut et al., 1983).

VI. PV mature protein $2C^{ATPase}$.

In poliovirus, $2C^{ATPase}$ is 329 amino acid long and, based on amino acid sequence analyses, it is classified as a member of the superfamily III helicases, which form hexameric ring structures (Gorbalenya and Koonin, 1993). Such proteins contain three conserved motifs, two of which are typical NTP-binding motifs (A+B) and the third one (C), downstream of motif B, contains an invariant asparagine preceded by a stretch of hydrophobic residues, but its exact function is unknown (FIGURE 5a). Downstream of

motif C is residue $N_{252}$, which is involved in the interaction with VP3 in a PV/CAV20 chimera (Liu et al., 2010). Poliovirus $2C^{ATPase}$ possesses ATPase activity *in vitro* (Mirzayan and Wimmer, 1994; Pfister and Wimmer, 1999; Rodríguez and Carrasco, 1993), which is inhibited by guanidine hydrochloride (GnHCl) (Pfister and Wimmer, 1999), a specific inhibitor of enterovirus RNA replication (Pincus et al., 1986). Numerous attempts to discover helicase activity have failed in the past although recently an RNA chaperone type activity was reported to be associated with the $2C^{ATPase}$ protein of EoV, a picorna-like virus (Cheng et al., 2013). Near its N-terminus, the protein contains an amphipathic helix (Paul et al., 1994b), an RNA binding domain (Rodríguez and Carrasco, 1995), a membrane binding domain (Echeverri et al., 1998) and an oligomerization domain (FIGURE 5a) (Adams et al., 2009). The central and C-terminal domains of the protein possess serpin (serine protease inhibitor) motifs and accordingly $2C^{ATPase}$ inhibits the proteinase activity of $3C^{pro}$ both *in vitro* and *in vivo* (Banerjee et al., 2004). Near the C-terminus the protein contains another amphipathic helix (Teterina et al., 1997) and a cysteine-rich $Zn^{++}$ binding domain (Pfister et al., 2000). The protein has the ability to oligomerize through sequences near its N-terminus (Adams et al., 2009) and to interact with viral proteins 2B/2BC, 3A/3AB, $3C^{pro}$, and VP3 (Banerjee et al., 2004; Cuconati et al., 1998; Liu et al., 2010; Yin et al., 2007) and cellular protein reticulon 3 (Tang et al., 2007). The 2BC precursor of $2C^{ATPase}$ also interacts with cellular protein VCP/p97 (Arita et al., 2012). A small RNA hairpin *cre* in the coding sequence of $2C^{ATPase}$ (FIGURE 5a) serves as template for the uridylylation of VPg during RNA synthesis (Goodfellow et al., 2000; Paul et al., 2000).

A study that inserted small DNA linkers to unique restriction sites implicated $2C^{ATPase}$ with uncoating. One of the recovered mutants virus had a small plaque phenotype and the other was defective in viral RNA synthesis (2C-31) (Li and Baltimore.,1988). Further passage of 2C-31 mutant resulted in an intragenic revertant mutant that had an uncoating defect at $32^o$C (Li and Baltimore.,1990). Single growth-curve at $32^o$C showed the reduction in titer compared to higher temperatures. Shifting infection incubation temperature to $39^o$C for 15 minutes before terminating in the infection changes yielded higher virus production. Since virus absorption of the mutant 2C-31 was higher than 90% of the total input, the authors concluded that the changes in nonstructural protein $2C^{ATPase}$ led to an uncoating defect. Interestingly, mutant virions were relatively stable, and showed resistance to heat and mild acid treatments similar to wild type. Additional passages resulted in mutations upstream and downstream of the linker insertion in $2C^{ATPase}$, which abolished the uncoating defect (Li and Baltimore.,1990).

The initial observation that linked $2C^{ATPase}$ to encapsidation came from experiments with hydantoin, a drug that inhibits virus growth at the stage of encapsidation (Vance et al., 1997). Drug resistant variants were identified that mapped to the N-terminal and central portions of the polypeptide (FIGURE 5b), but there was no clear correlation between these sites and other known motifs (Vance et al., 1997; Wang et al., 2012). Early genetic studies also indicated the involvement of $2C^{ATPase}$ in encapsidation. A *ts* mutant with an insertion in $2C^{ATPase}$ yielded suppressor mutations that resulted in a cold sensitive uncoating defect (Li and Baltimore, 1990). This finding suggested that $2C^{ATPase}$ has a role in determining some aspect of virion structure. Our

charged to alanine scanning mutagenesis, noted above, has revealed that residues

$K_{279}/R_{280}$ near the C-terminus of the protein in a $Zn^{++}$ binding domain are also required

for encapsidation (Wang et al., 2012). In addition, we identified a *ts* mutant

$(C_{272}A/H_{273}A)$, also in the $Zn^{++}$ binding domain of the protein, that was defective in

encapsidation (Wang et al., 2014). The delayed growth kinetics of this virus suggested

the possibility of an additional uncoating defect.

**FIGURE 1. Phylogenetic tree of *Picornaviridae*.** *Picornaviridae* virus family contains 26 genera and growing. Eight current genera (shown in bold), 4 current proposals (shown in quotations), and one unnamed genus proposal in preparation. PV belongs to the Enterovirus genus (combined with coxsackie A virus [in red]). The figure is modified from www.picornastudygroup.com/poster/**europic_2008**.pdf

"Porcine sapelovirus"

"Avian sapelovirus"

"Simian sapelovirus"

*Teschovirus*

*Porcine teschovirus*

*Cardiovirus*

*Encephalomyocarditis virus*

*Theilovirus*

"Senecavirus"

"Seneca Valley virus"

"Human rhinovirus C"

*Human rhinovirus B*

*Human rhinovirus A*

*Human enterovirus C*

Coxsackie A virus / Poliovirus

*Simian enterovirus A*

*Bovine enterovirus (B)*

*Bovine enterovirus (A)*

*Porcine enterovirus B*

*Human enterovirus D*

"Simian enterovirus B"

*Human enterovirus A*

*Enterovirus*

*Equine rhinitis B virus*

*Erbovirus*

*Equine rhinitis A virus*

*Aphthovirus*

*Foot-and-mouth disease virus*

"Bovine rhinitis B virus"

*Kobuvirus*

*Aichi virus*

*Bovine kobuvirus*

*Hepatovirus*

*Hepatitis A virus*

"Avian encephalomyelitis virus"

"Tremovirus"

*Parechovirus*

*Ljungan virus*

*Human parechovirus*

"Duck hepatitis A virus"

"Seal picornavirus 1"

Unnamed

"Avihepatovirus"

0.2

**FIGURE 2. Poliovirus genome organization and functional motifs in the PV 2C$^{ATPase}$ protein.** PV RNA contains a long 5' nontranslated region (5'NTR), a single open reading frame, a short 3'NTR, and a poly(A) tail. The single open reading frame is translated into a polyprotein that is processed by virally encoded proteinases 2A$^{pro}$ (diamond) and 3C$^{pro}$/3CD$^{pro}$ (triangle). The stars indicate the cleavage rates, where more stars indicate fast cleavage. The maturation cleavage (shown as "question mark") occurs by unknown mechanism. The structure of the *cre* element, located in the coding sequence of protein 2C$^{ATPase}$, is also shown.

POLYPROTEIN

| P1 | P2 | P3 |
|---|---|---|
| VP0(4,2)31 | 2ABC | 3ABCD |

| VP0 | VP3 | VP1 | 2A^pro | 2BC | 3AB | 3CD^pro |
|---|---|---|---|---|---|---|

***   ***   ***   ***

?

| VP4 | VP2 | VP3 | VP1 | 2B | 2C^ATPase | 3A | 3C^pro | 3D |
|---|---|---|---|---|---|---|---|---|

VPg

\*   \*
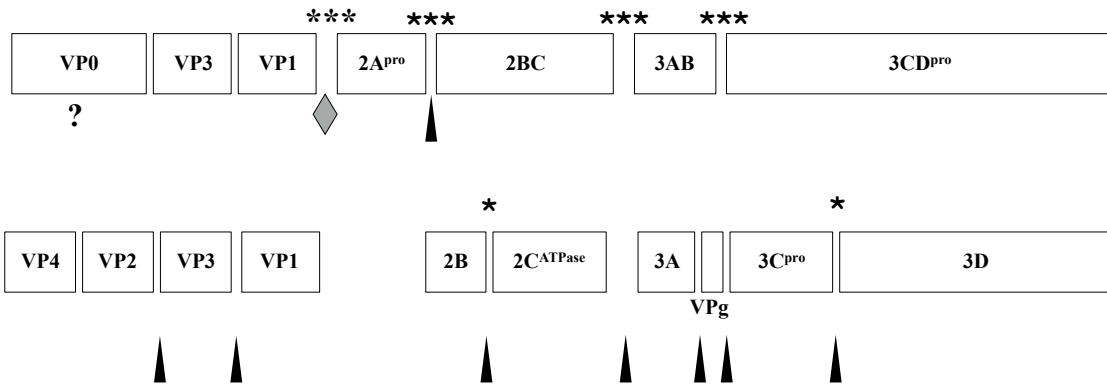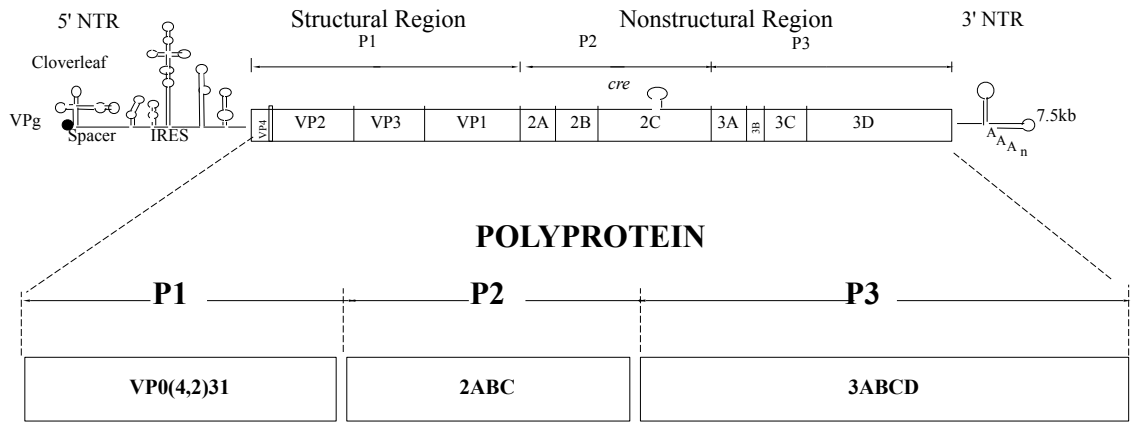
◊   2A^pro catalyzed

▲   3C/3CD^pro catalyzed

**FIGURE 3. Circulating Vaccine Derived Polioviruses (cVDPVs) occurrences in different parts of the world.** cVDPV's of type 1, type 2, and type 3 are highlighted box in red, yellow, and blue respectfully. Countries of isolated viruses are on top, then followed by the serotype and year/s of virus isolates, and blow is the number of reported cases. Data was acquired from WHO headquarters in 2010.

Afghanistan
Type 2, 2010
3 cases

China
Type 1, 2004
4 cases

Ethiopia
Type 2, 2008-09
4 cases

Type 3, 2008-09
4 cases

Egypt
Type 2, 1988-93
30 cases

Myanmar
Type 1, 2006-07
5 cases

Nigeria and Niger
Type 2, 2005-10
316 cases

Cambodia
Type 3, 2005-06
2 cases

Hispaniola
Type 1, 2000-01
21 cases

Philippines
Type 1, 2001
3 cases

Guinea
Type 2, 2009
1 cases

Indonesia
Type 1, 2005
46 cases

DR Congo
Type 2, 2008-10
21 cases

Madagascar
Type 2, 2001-02
5 cases
Type 2 and 3, 2005
5 cases

Somalia
Type 2, 2008-9
5 cases

India
Type 2, 2009-10
15 cases

Type 1
Type 2
Type 3

**FIGURE 4. $C_{20}PP$ chimera viruses are rescued by mutations in $2C^{ATPase}$ or/and in VP3.** Growth phenotypes of the $C_{20}PP$ chimera and of its derivatives. The genomic structures of CAV20 and chimera $C_{20}PP$ virus and of its derivatives are illustrated on the left. The amino acid changes in $2C^{ATPase}$ and in VP3 are shown in superscript. $C_{20}PP$-$(E_{180}G + N_{252}S)$ represents a chimeric mutant virus with the double mutations $(VP3^{(E180G)}$ and $2C^{ATPase\ (N252S)}$. $C_{20}PP$ was shown to have an encapsidation defect (Liu et al., 2010).
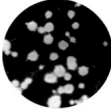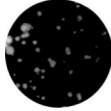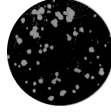
| | CPE | Virus titer Log$_{10}$PFU/ml | Plaque phenotype |
|---|---|---|---|
| **CAV20** | 0 passage | 8.4 | |
| **C$_{20}$PP** | 3$^{rd}$ passage | 5.1 | |
| **C$_{20}$PP-(2C$^{N252S}$)** | 0 passage | 5.0 | |
| **C$_{20}$PP-(VP3$^{E180G}$)** | 0 passage | 5.3 | |
| **C$_{20}$PP-(E$_{180}$G + N$_{252}$S)** | 0 passage | 7.8 | |

**FIGURE 5. Functional motifs, encapsidation mutations and uncoating mutations in PV 2C$^{\text{ATPase}}$ protein.** (a) The locations of the known functional domains of the 2C$^{\text{ATPase}}$ protein are noted. (b) Previously identified mutations in 2C$^{\text{ATPase}}$ involved in encapsidation or uncoating are shown in detail. These include the hydantoin resistant mutations, N252 the capsid interacting site in the PV/CAV chimera, the residues involved in encapsidation derived from alanine scanning mutagenesis and the mutations leading to an uncoating defect in a mutant containing a nearby linker insertion.

**(a)**

Oligomerization 1–38
Membrane binding 21–54
RNA binding 21–45
Amphipathic helix 10–32

108-128 · *cre* · 129-136 **A** · NTP binding & hydrolysis · 172-177 **B** · 217-223 **C** · 269 – 286 cysteine-rich zinc-binding · RNA binding 290–309 · Amphipathic helix 312–319

1 — 329

**(b)**

Q65 · L125 · **A** · **B** · **C** · V218 · N252 · K259 (C272/H273) · (K279/R280) · cysteine-rich zinc-binding · M293 · K295

1 — 329

✡ Hydantoin/encapsidation ◆ Capsid interacting ◇ Encapsidation ◆ Uncoating ⬡ Encapsidation/Uncoating

27

**SPECIFIC AIMS**

Poliovirus (PV), one of the best studied plus strand RNA viruses, belongs to the genus *Enterovirus* of the *Picornavaridae* family. Even though PV is considered the prototype of the *Enterovirus* genus, very little is known about the details of virion morphogenesis, the last step in virus replication during which the viral RNA is enclosed in a protective coat. Nonstructural PV protein $2C^{ATPase}$ is known to play an essential role in viral morphogenesis. This multifunctional protein is also involved in many other important steps of the viral life cycle, such as virus uncoating, host cell membrane binding and rearrangement, the induction of viral cytoplasmic replication vesicles, RNA binding and RNA synthesis. An in depth knowledge of the functions of $2C^{ATPase}$ will contribute to our understanding of the molecular biology of poliovirus. Recent studies from our laboratory have shown that in a PV/coxsackie A virus (CAV) chimera PV $2C^{ATPase}$ provides the specificity of encapsidation through an interaction with capsid protein VP3 of CAV20, through residue $N_{252}$ of $2C^{ATPase}$.

My first goal was to determine a structural model of the $2C^{ATPase}$ polypeptide that could be used to design potential encapsidation mutations near the capsid interacting site for our genetic studies. In addition, a structural model can be used to insert tags into the polypeptide that will likely not affect viral growth. Remarkably, the crystal structure of $2C^{ATPase}$ has not yet been solved because the membrane bound mature protein cannot be isolated in a soluble form. In this study, I predicted the protein structure of $2C^{ATPase}$ using a Phyre2 protein structure predicting server. Based on the predicted structure, I investigated the susceptibility of $2C^{ATPase}$ to small tag insertions. I generated and

analyzed the tagged $2C^{ATPase}$ mutant viruses. The usefulness of the inserted tags was demonstrated by immunofluorescent imaging.

My next goal was to search for additional sites in $2C^{ATPase}$ near $N_{252}$, the capsid interacting site that might be involved in morphogenesis. Previous work from our laboratory has demonstrated an essential interaction between CAV capsid protein VP3 ($E_{150}G$) and PV $2C^{ATPase}$ ($N_{252}S$) for encapsidation in the context of a chimeric PV and CAV20 virus. Interestingly, in the PV background $N_{252}$ can be changed into serine or glycine ($N_{252}{\rightarrow}S$ or G) without any effect on viral growth. Therefore I searched for other residues in the vicinity of $N_{252}$ that might facilitate PV encapsidation.  In this study, I designed and constructed 5 alanine mutants on the basis of the modeled $2C^{ATPase}$ structure. Some of the mutations were lethal in tissue culture and others carried conditional defects. A cold sensitive mutant ($K_{259}A$) was analyzed in more detail and was found to be defective both in encapsidation and in uncoating during the next cycle of infection.

**MATERIALS AND METHODS**

I. *In silico* analysis of PV 2C^ATPase

I used a bioinformatics server that utilizes a protein homology and fold

recognition algorithm called Phyre2, Protein Homology/analogy Recognition Engine V

2.0 (Phyre2), to predict the structure of poliovirus 2C$^{ATPase}$ (Kelley and Sternberg, 2009).

The amino acids sequence of PV 2C$^{ATPase}$ was submitted to the Phyre2 web server

(http://www.sbg.bio.ic.ac.uk/phyre2) to search for a suitable query sequence coverage

and sequence identity.

The predicted 3D model structure was analyzed with using the educational

version of PyMOL software (The PyMOL Molecular Graphics System, Version 1.0

Schrödinger, LLC). Generation of the 2C$^{ATPase}$ hexamer Super-positioning model was

performed with combination of softwares; TextEdit was used to modify the coordinate of

various amino acid positions. Visual molecular Dynamics software was used to perform

protein structure alignments as well as super-positioning coordination of a recA hexamer.

Electrostatic representations were performed with pyMOL. In addition, all images were

also acquired with pyMOL software.

II. HeLa R19 cells cultures

Adhesion HeLa R19 cells were maintained in Dulbecco minimal Eagle medium

(DMEM, Life Technology) that was supplemented with 10% bovine calf serum (BCS)

and 100 units of penicillin and 100 μg of streptomycin. Transfected and infected HeLa

cells were incubated with 2% BCS. Cells were incubated at 37$^{o}$C in 5% $CO_2$.

III. Plasmids

The pT7PVM plasmid contains the full-length infectious cDNA of PV1(Mahoney) that has an engineered *EcoR1* restriction site downstream of the viral 3'NTR. pT7R-Luc-PPP is an infectious Renilla luciferase reporter virus construct in which the 311 amino acids long R-Luc polypeptide is expressed as an N-terminal fusion between the 5'NTR and the PV polyprotein (Liu et al., 2010).

## IV. Site directed mutagenesis

The standard site-directed mutagenesis protocol was used to obtain the desired mutations for both the triple alanine and single alanine mutants of PV 2C$^{ATPase}$. Mutated nucleotides and their corresponding amino acid(s) are summarized in Tables 2 and 3. In each case, the desired residues were replaced with alanine by changing the corresponding codons. An *Xho*I/*Hpa*I fragment, spanning parts of the 2C$^{ATPase}$ and 3A coding regions, was used as template for site-directed mutagenesis. The mutated sites and corresponding codon changes are summarized in Tables 1 and 2. After sequencing analysis the designed 2C$^{ATPase}$ mutations were independently subcloned into pT7PVM, or the Renilla luciferase reporter virus plasmid (R-Luc-PPP).

## V. Preparation of RNA transcripts.

Wt and mutant constructs were linearized at a unique sites for both pT7PVM and R-Luc-PPP constructs, *EcoRV* and *PvuII*, respectively. Linear constructs were used as templates for *in vitro* RNA synthesis using T7 RNA polymerase.

## VI. Transfection of RNA into HeLa cells

RNA transcripts (3-10 μg) were transfected into 35-mm-diameter HeLa R19 cell monolayers by the DEAE-Dextran method, and incubated at indicated temperatures.

## VII. In vitro translation using HeLa cell free extract

31

HeLa S10 cells S10 cytoplasmic were prepared as previously described (Molla, Paul 1991). HeLa cellular extracts were modified in this experiment. In terms of nuclease treatment, HeLa extracts were immediately treated with nuclease (1U/ μl)/200 μl after removal of the cellular nucleus and cellular debris. Nuclease treated-HeLa extracts were gently vortexed and incubated at room temperature for 15 minutes.  Then, 6 μl of 100 mM EGTA was added to every 200 μl of extract and vortexed gently.

2. Master mix:

150 μl nuclease treated Hela extract

50 μl translation mix

22 KAc 2M (0.1M final)

3 μl M μl gAc 50 mM (0.35mM final)

16 μl MgCl2 (20 mM final)

25 μl $^{35}$S-methionine

266 μl –Final volume that is sufficient for over thirty translation reactions

3. Translation reaction:

8.8 μl master mix

2.7 μl RNase free water

1.0 μl of respective viral RNA in RNase free water

Incubate at 34$^o$C overnight

VIII. Virus purification

Wt PV viruses and $K_{259}A$ mutant viruses were propagated in HeLa R19 on nine 60 mm plates in order to generate enough virus for cesium-chloride (CsCl) purification.

IX. Plaque assays

Plaque assays were performed on HeLa R19 monolayers using 0.6% tragacanth gum. After 72 hr of incubation at 33$^{\mathrm{o}}$C or 48 hr of incubation at 37$^{\mathrm{o}}$C or 39.5$^{\mathrm{o}}$C, the viral plaques were developed with 1% crystal violet (Molla et al., 1991).

X. RT-PCR and sequencing analysis of viral RNAs isolated from plaque-purified viruses

RNA was extracted from 200 μl lysate with 800 μl Trizol reagent (Invitrogen) and reverse transcribed into cDNA using SuperScript III reverse transcriptase (Invitrogen). PCR products were generated using high fidelity Fusion polymerase (Finnzyme). PCR products were purified and further sequenced.

XI. Luciferase assays

Monolayer HeLa R19 cells were independently transfected with 3-5 μg of R-Luc-PPP reporter virus transcript RNAs derived from cDNAs linearized with *Pvu*I. The transfected cells were incubated at 33$^{\mathrm{o}}$C, 37$^{\mathrm{o}}$C, and 39.5$^{\mathrm{o}}$C overnight in DMEM with 2% (v/v) BCS in the presence and absence of 2 mM GnHCl. Luciferase activity was determined on the cell supernatants after three freeze-thawing steps. Cell supernatant (100 μl) were mixed with 20 μl renilla luciferase assay reagent (Promega luciferase assay system; catalog # E2810), and R-Luc activity were measured in an OPTOCOM I luminometer (MGM Instruments, Inc.). Two hundred fifty μl cell supernatants from transfections in the absence of GnHCl were passaged once in the presence and absence of 2 mM GnHCl. Luciferase activity was determined in the supernatants after an overnight incubation. The R-Luc ratio was calculated as: luciferase activity without GnHCl divided by luciferase activity with GnHCl in transfection or infection (-GnHCl/+ GnHCl).

XII. Immunoblot assay

Monolayer HeLa R19 cells were independently infected at a multiplicity of infection (m.o.i.) of 5 with wt and $K_{259}A$ viruses and incubated at $33^{o}C$, $37^{o}C$, and $39.5^{o}C$. The growth media were aspirated at 3 hr, 5 hr, 6.5 hr, and 8 hr, respectively, and cells were lysed with triton X-100 detergent. Cell lysates from the various time points were seperated on an SDS-PAGE gel and transferred to a nitro-cellulose membrane. $2C^{ATPase}$ protein and VP3 (capsid protein) were detected using primary mouse monoclonal and rabbit polyclonal antibodies, respectively.

## XIII. Immunofluorescence

HeLa R19 cells were infected with wt or $K_{259}A$ virus at an m.o.i. of 5 and incubated at $37^{o}C$ for 4 hr, $35^{o}C$ for 5 hr, or $33^{o}C$ for 6 hr. Cells were fixed with 4% para-formaldehyde for 15 minutes at room temperature. Then the cells were permeabilized with 0.2% Saponin and probed for mature virus with A12 primary antibody, which exclusively recognizes PV mature virus, and secondary Alexa Fluor 488-conjugated antibody. The localization of $2C^{ATPase}$ was determined in the same cell using monoclonal $2C^{ATPase}$ antibody and an Alexa Fluor 555-conjugated secondary antibody. Images were taken with Nikon's super-resolution 3D-structured illumination microscopy (SIM).

## Preparation for imaging

HeLa R19 cells were grown on glass slide overnight and infected at various time points the next day. Cell medium were removed and fix with 4% paraformaldehyde for 20 minutes on ice. Cells were washed three times for 5 minutes each in PBS on ice. For longer-term storage, samples were stored in PBS + sodium azide at $4^{o}C$. PBS PBS with

sodium azide were aspirated from cells. Fixed cells were block for 1 hour in PBST [(PBS + 0.2% triton) + 5% BSA +5% goat serum at room temperate. Then cells were incubated overnight in respective primary antibody in blocking solution without serum at 4$^o$C overnight. Cells were washed three times in PBS for 5 minutes each. Wash numbers were increased to five times for VP3 primary antibodies to reduce the background. Fixed cells were incubated for 1 hour with secondary antibody in blocking solution without serum at room temperature in the dark. Cells were washed three times in PBS for 5 minutes each in the dark. Immuno-stained cells were incubated with DAPI for 30 seconds to 2 minutes at room temperature and washed two times in the dark at room temperature. Cell culture glass was mounted using fluoromount G mounting oil.

**TABLE 1:  List of primers.**

Primers 1 and 2 were used for the generation of 2C$^{\text{ATPase}}$ tag-inserted constructs; PV1(M) 2C-strepII tag  and PV1(M) 2C-FLAG tag, described in chapter 1. Primers 3-6 were used for the generation of triple alanine mutations mutant constructs in chapter 2. Primers 7-11 were used for the generation of single alanine mutant constructs, also described in chapter 2 experiments. Primers 12-13 were used for quantitative RT-PCR to measure RNA levels. Nucleotides in bold are in italic and bold and were changed from the original PV sequences to the corresponding mutations.

| No. | PRIMER NAME | SEQUENCE |
|---|---|---|
| 1 | 2C-strepII | F- ***TGGAGCCACCCGCAGTTTGAA***AAGAGATGCTGTCCTTTAGTGTGTGG<br>R- CTT***TTCAAACTGCGGGTGGCTCCA***GTTTGCTGGTTGGTGACAGTTCTT |
| 2 | 2C-flag | F- ***GACTACAAAGACGATGACGAC***AAGAACTGTCACCAACCAGCAAACTTTAAGAGATGC<br>R- CTT***GTCGTCATCGTCTTTGTAGTC***ACACATTTCAGTAGCCATGGCCATGTTCAATTTCC |
| 3 | QVM/AAA | F- GACATGGACATT***GCGGCCGCC***AATGAGTATTCTAGAGATGG<br>R- CTCTAGAATACTCATT***CGCCGGCGG***AATGTCCATGTCGAACGC |
| 4 | EYS/AAA | F- CATTCAGGTCATGAAT***GCGGCTGCT***AGAGATGGGAAATTGAACATGG<br>R- CAATTTCCCATCTCT***AGCAGCCGC***ATTCATGACCTGAATGTCC |
| 5 | GKL/AAA | F- TGAGTATTCTAGAGAT***GCCGCAGCC***AACATGGCCATGGCTACTG<br>R- AGCCATGGCCATGTT***GGCTGCGGC***ATCTCTAGAATACTCATTC |
| 6 | FMI/AAA | F- GCCAGGCGCTTTGCG***GCC***GAC***GCG***GAC***GCT***CAGGTCATGAATGAGTATTC<br>R- ACTCATTCATGACCTG***AGC***GTC***CGC***GTC***GGC***CGCAAAGCGCCTGGCTAACG |
| 7 | F$_{244}$A | F- GCCAGGCGCTTTGCG***GCC***GACATGGACATTCAGGTCATGAATGAG<br>R- CTCATTCATGACCTGAATGTCCATGTC***GGC***CGCAAAGCGCCTGGC |
| 8 | M$_{246}$A | F- GCCAGGCGCTTTGCGTTCGAC***GCC***GACATTCAGGTCATGAATGAG<br>R- CTCATTCATGACCTGAATGTC***CAT***GTCGGCCGCAAAGCGCCTGGC |
| 9 | I$_{248}$A | F- GCCAGGCGCTTTGCGTTCGACGCCGAC***ATT***CAGGTCATGAATGAG<br>R- CTCATTCATGACCTG***AAT***GTCCATGTCGGCCGCAAAGCGCCTGGC |
| 10 | K$_{259}$A | F- GAATGAGTATTCTAGAGATGGG***GCA***TTGAACATGGCCATGGCTAC<br>R- GTAGCCATGGCCATGTTCAA***TGC***CCCATCTCTAGAATACTCATTC |
| 11 | L$_{260}$A | F- GAATGAGTATTCTAGAGATGGGAAAGCAAA***CAT***GGCCATGGCTAC<br>R- GTAGCCATGGCCATGTT***TGC***TTTCCCATCTCTAGAATACTCATTC |
| 12 | P1 | F- ACCCTTCCAAGTTCACCGAG<br>R- TACCCGCAAGCCTCTATGTT |
|  | GAPDH | F- TGCACCACCAACTGCTTAGC<br>R- GGCATGGACTGTGGTCATGAG |

## Chapter 1: Prediction of poliovirus 2C$^{ATPase}$ 3D structural model and characterization of tag-inserted viruses

**RESULTS**

I. PV 2C$^{ATPase}$ three-dimensional structure prediction

Studies of the role of 2C$^{ATPase}$ in encapsidation have been hindered by the multifunctional nature of the protein (Wang et al., 2012) as well as by the stringent dependence *in cis* of translation>RNA replication>assembly (Paul and Wimmer, 2015; Wang et al., 2012). Despite considerable studies of the functions of this protein in the viral life cycle, little information is available about its secondary structure and none about the three dimensional structure. A three-dimensional structure would provide better insights into its function in morphogenesis. The propensity of 2C$^{ATPase}$ to bind to membranes has thus far prevented the purification of the polypeptide in a soluble form and consequently its three dimensional structure has not yet been determined. Only the GST- and MBP-tagged full-length PV 2C$^{ATPase}$ polypeptides or the protein anchored to small Nano disk membrane bilayers have been obtained in soluble forms (Adams et al., 2009; Pfister and Wimmer, 1999; Springer et al., 2013). The development of bioinformatic tools predicting protein structure is constantly evolving. The availability of such *in silico* approaches provides cost saving and less time consuming paths to investigate protein functionality than that of conventional experimental methods.

I used Phyre2 to predict a query model of PV 2C$^{ATPase}$ structure. The server generated a model structure that was modeled after chain C of transport protein vcp/p97 in a complex with ADP/ADP (protein database number 3CF1). Phyre2 predicted a 2C$^{ATPase}$ structure for 92% of the residues with greater than 90% confidence in the

modeled polypeptide (FIGURE 6). In addition, the model had 100% confidence in 92%

of the 329 residues of $2C^{ATPase}$. The N-terminal segment, highlighted in black, is highly

unreliable while sequences highlighted in light brown can be predicted with good

confidence (FIGURE 6a). The remainder of the sequence, shown in light green, is

predicted with 100% confidence.

The predicted $2C^{ATPase}$ model can be subdivided into three structured domains (N-

terminal, central helicase, and C-terminal) connected by flexible regions (FIGURE 1b).

The N-terminal domain (red) contains helical regions. It should be noted that within this

region the removal of the amphipathic helix (residues 1 to 33), which affects membrane

binding, was found to be sufficient for the production of truncated soluble FMDV

$2C^{ATPase}$ protein (Sweeney et al., 2010). The central domain (blue) contains the conserved

NTP binding boxes (yellow) A, B of all helicases and box C, specific for SF3 helicases

(Gorbalenya and Koonin, 1993). Phyre2 predicted the structure of this domain with 100%

confidence to contain both α helices and β sheet secondary structures. The C-terminal

domain contains the cysteine rich $Zn^{++}$ binding domain that is already known to be

involved in encapsidation (Wang et al., 2014; 2012).

II. Protein contact potential and super-positioning analysis

It has been previously shown that $2C^{ATPase}$ oligomerizes to form a hexamer, like

other well-known AAA+ ATPases (Adams et al., 2009). The oligomerization domain of

the protein was identified to be near the N-terminus in an amphipathic helix.  In this

study, I performed a protein contact potential analysis, which predicts the binding affinity

potential of peptides of a protein structure was performed on the $2C^{ATPase}$ model using

PyMOL (v 1.0) (FIGURE 7). The $2C^{ATPase}$ structure reveals clusters of charged residues

around the protein, which is a characteristic of proteins that oligomerize. We did not perform additional analysis on the previously identified oligomerization domain (Adams et al., 2009) because the phyre2 predicted structure of this domain in $2C^{ATPase}$ was highly unreliable. Interestingly, the electrostatic representation of the ATPase domain had a positively charged pocket and a negatively charged region protruding behind at the opposite side of the structure. Such protein contact analysis suggests that the two polar sides may potentially contact each other in a homo-oligomerization structure. In addition, there is a highly positively charged pocket between the ATPase region and the C-terminal domain that is in close vicinity of the $2C^{ATPase}$'s capsid interacting site (FIGURE 7).

To gain some structural insight into the putative $2C^{ATPase}$ hexamer's functionality, we performed super-positioning alignment of the phyre2 model to recA hexamer (pdb:2rec) (Yu and Egelman, 1997) (FIGURE 8). RecA is a 38 kDa ATPase protein that has essential roles in DNA repair and recombination. The generated $2C^{ATPase}$ superposition model has a core pore that is 23 Angstroms (Å) in diameter, which would make it permissive for single stranded or double stranded RNA to pass through. Moreover, electrostatic representation of the $2C^{ATPase}$ hexamer showed two amino acids that directly point to the center of the hexamer core (Lysine 168 and Arginine 226) (FIGURE 8a). The two charged amino acids are 13 Å from each other in the structure. Interestingly, the front and back interfaces in the hexameric model are primarily composed of the N-terminal and the C-terminal amino acids of $2C^{ATPase}$, respectively (FIGURE 7, FIGURE 8 a and b). The front and side interfaces are primarily composed of more positively charged peptides than the back interphase, which contains more negatively charged peptides (FIGURE 8 a-c). The superposition model also shows that

the previously identified oligomerization domain of 2C$^{ATPase}$ (Adams et al., 2009) is not in direct contact in the context of our hexameric model.

III. Structure based prediction of insertion sites in PV 2C$^{ATPase}$

A previous high throughput transposon screen identified different sites in PV nonstructural proteins that could tolerate small peptide insertions (Teterina et al., 2011) . Surprisingly, the screen was able to identify sites in all nonstructural proteins with the exception of 2C$^{ATPase}$.  Since I generated a high confident protein structure, I attempted to use the information from the predicted structure to generate a tagged 2C$^{ATPase}$ virus that would facilitate in the identification of proteins, both viral and cellular, that complexes with PV 2C$^{ATPase}$. Recent studies have used such an approach to identify viral and host proteins that form complexes with viral RNA (Lenarcic et al., 2013).

Insertion of tag epitopes in viral proteins are particularly difficult for small viruses because the insertion can interfere with the final folding of the mature protein or the processing of the precursor polypeptide, which can interfere with virus viability, in terms of growth. I identified two susceptible peptide insertion sites in PV 2C$^{ATPase}$ based on the criteria that they mapped in the flexible unstructured region of the protein and that phyre 2 predicted the structure of this domain with the highest confidence (FIGURE 9). These sites were located near the C-terminus of the protein in a Zn++ binding domain outside of the ATPase domain or the predicted hexameric structure of the polypeptide.

IV. Characterization of PV mutant viruses tagged in 2C$^{ATPase}$

The sequence that codes for the StrepII and FLAG tags were independently inserted into two sites, selected by structure based prediction (FIGURE 9) in pT7PV1(M) cDNA. Constructs were linearized, transcribed into RNA using T7 polymerase and

transfected into HeLa cells. Cells were passaged up to 10 times on HeLa cells or until viable virus was recovered. I was not able to recover viruses from the second site insertions (site II). However, viable mutant viruses were recovered from both the strepII and FLAG tag insertions at site I (FIGURE 9). PV 2C-tagged mutant viruses were recovered after the second and sixth passage for the strepII and FLAG inserted mutants, respectively (FIGURE 10). The PV 2C-strepII mutant virus had similar growth kinetics to that of the wt and also produced high virus titers after six hours infection (FIGURE 10a). The plaque phenotype of the PV-2C-strepII was smaller than that of the wt. In contrast the PV-2C-FLAG mutant virus that had a wt-like plaque phenotype (FIGURE 10b).

Sequence analyses of the full-length genomes of the recovered tag-inserted mutants revealed suppressor mutations. Two independent suppressor mutations were recovered from the PV-2C-strepII tag mutant sequence analysis, methionine at position 264 to lysine ($M_{264}K$) and an isoleucine to leucine at position 310($I_{310}L$) (FIGURE 11) of $2C^{ATPase}$. A single nucleotide change converted the original amino acids to the suppressor genotype in both suppressor mutants. Surprisingly, we recovered a suppressor mutation that maps to mature protein 2B in the PV-2C-FLAG tagged mutant virus. This was also a single nucleotide change resulting in the exchange of a nearly neutral residue theronine with a hydrophobic residue isoleucine ($T_3I$). In addition, the sequence analysis also revealed an additional suppressor mutation that mapped to the FLAG epitope (FIGURE 11). The mutation resulted from a single nucleotide change in the last codon of the tag of a negatively charged aspartic acid to a hydrophobic glycine (D→G).

V. Tagged epitope recognition of $2C^{ATPase}$ tagged viruses

Wt PV and PV-2C-tagged mutant viruses were used to infect HeLa cells for 4 hr and 5 hr, for wt and tagged mutants, respectively, and the cell lysates were analyzed on SDS-polyacrylamide gels. Western analysis with antibody to $2C^{ATPase}$ detected the tagged $2C^{ATPase}$ proteins. Moreover, antibodies to the strepII and FLAG epitopes were also detected the tagged 2C proteins (FIGURE 12). Next, cells were infected with the PV-2C-FLAG tagged mutant virus for 4 hours of incubation. Immuno-florescence imaging was performed using antibodies against $2C^{ATPase}$ and FLAG peptide (FIGURE 12 and 13). Though the mutant PV $2C^{ATPase}$ FLAG epitope has a suppressor mutation in it the FLAG epitope, the antibody successfully detected the tag both in western and imaging analyses. To summarize, the epitopes in the PV-2C-tagged viruses are recognized by their respective antibodies, and will be useful tools for biochemical studies such as the identification of viral or host cellular factors that interact with $2C^{ATPase}$ during replication or morphogenesis.

**DISCUSSION**

The studies in this chapter demonstrate the feasibility of using structure prediction models to obtain useful biological information. In my case, I predicted the structure of PV $2C^{ATPase}$ based on its homology with vcp/p97 protein and I also successfully generated a hexameric model of the putative helicase structure. More importantly, the analysis of the PV-$2C^{ATPase}$ structure resulted in the identification of a site in the protein that tolerated tag epitope insertion. I recovered two independent viable mutant viruses that proved useful for biochemical assays of $2C^{ATPase}$ function.

The difficulties in purifying large amounts of $2C^{ATPase}$ in solubilized forms have so far hindered crystallization attempts. $2C^{ATPase}$ is a membrane bound protein and its association with membranes is through an amphipathic helix that is located near its N-terminus (Paul et al., 1994b). Previous studies with the $2C^{ATPase}$ of another picornavirus, foot-and-mouth disease virus have found that removal of the N-terminal membrane binding region increased the yield of solubilized protein (Sweeney et al., 2010). Another study used nanodiscs to generate soluble forms of $2C^{ATPase}$ with increased ATPase activity (Springer et al., 2013); however, none of these strategies have yielded any structural data. I bypassed the $2C^{ATPase}$ solubility complication by using an algorithm that predicted its structure based on its homology to other protein structures, which resulted in a high confidence model. Not surprisingly, the server produced a highly unreliable model for the N-terminal membrane-binding region of the protein (FIGURE 6). In addition, I also modeled the charges on the surface peptides, which suggests that the oligomerization of the protein can result from polar contacts of the ATPase domain (FIGURE 7). It was previously shown that the N-terminal membrane-binding domain was necessary for

44

oligomerization, but our model suggests that these regions do not directly contact each other. The possibility exists that the polar sides require monomers to be in close proximity to oligomerize, and membrane binding may facilitate this process.

One of the very interesting findings in the modeling was the putative hexamer with a positively charged core. The core has lysines and arginines protruding to the center. The positively charged core suggests the possibility that it interacts with a negatively charged molecule like the RNA. Also the diameter of the core is large enough to accommodate both double and single stranded RNA. In our superposition analysis, we followed the recA model, however, there are rooms for tighter fitting of the hexamer that would reduce the core, which may allow the penetration of a single RNA strand.

Studies of cellular localization, the composition of replication complexes, or the isolation of interacting partners of 2C$^{ATPase}$ are lacking and would be easier with a small tag epitope inserted into a functional viral protein. Site that are tolerable for small amino acids have been identified for all non-structural proteins of PV using transposon screens, with the exception of 2C$^{ATPase}$ (Teterina et al., 2006). Previous studies have inserted small DNA linker into the 2C$^{ATPase}$ through an inserting linker screen in 2C$^{ATPase}$ (Li and Baltimore, 1990; 1988). In my experiments both insertion tolerable sites were located between the ATPase domain and the C-terminal domain. I identified two sites that could potentially permit insertion of tag peptides that are larger than the previously inserted stretch of amino acids. I was able to recover 2C$^{ATPase}$ tagged mutant virus from one of the sites (site I) that is located in the beginning of the cysteine-rich zinc-binding region. I took advantage of a lysine at the site and incorporated it into the tag, since both the strepII and FLAG tags end with a lysine. The second site, which was downstream of the

45

cysteine-rich zinc-binding region, did not yield any viable viruses even after 10 passages, though the second site (site II) maps to a flexible unstructured region. Insertion sites always localize to flexible unstructured regions, however, not all flexible regions of tolerate insertions. The failure to recover viable mutants from the Site I indicates that selecting an unstructured region alone cannot be used as the only determinant of an insertion site. Some studies suggest that the variability of the amino acids could also correlate with their susceptibility for insertion (Egger et al 2000).

It took at least two passages to yield a PV-2C-tagged mutant virus. Sequence analysis showed that the PV-2C-strepII tagged mutant viruses generated suppressor mutations. Both mutations were located in the $2C^{ATPase}$ protein, one with a change of a hydrophobic methionine ($M_{246}$) to a positively charged lysine and the other an isoleucine ($I_{310}$) to leucine. The StrepII epitope, which is neutrally charged, might affect the overall charge of the surrounding region in the protein, and might be in part compensated by the suppressor mutations. The impact of the strepII insertion on viral growth was most noticeable on the plaque size that is smaller than that of the wt (FIGURE 10). However, the PV-2C-FLAG tagged mutant virus yielded high titers, with wt-like kinetics and exhibited a wt-like plaque phenotype, though the epitope peptide contains negatively charged amino acids. Sequence analysis showed that the viable mutant had a single nucleotide change that changed an aspartic acid to a glycine. The mutation to the hydrophobic glycine residue might have been selected by the virus to reduce the overall charge at that position (FIGURE 11). Fortunately, the mutated FLAG tagged epitope was still recognized by an antibody against FLAG in both western and immuno-fluorescence assays (FIGURE 12 and 13). Sequence analyses also revealed a second mutation that

mapped to PV viral protein 2B (FIGURE 11). This mutation suggests a direct contact between insertion site I and the N-terminus of 2B, either at the level of precursor 2BC or the mature 2B. It is interesting to note that results of a previous study demonstrated that a $2C^{ATPase}$ amphipathic helix chimera of PV with HRV14 yielded suppressor mutations near the N-terminus of 2B, again suggesting a functional interaction between 2B and $2C^{ATPase}$ (Teterina et al., 2006). These protein/protein interactions were confirmed by mammalian cell two-hybrid analyses.

Our *in silico* analysis yielded useful insights into the structure of $2C^{ATPase}$ and generated mutant viruses that can be used to perform biochemical studies or identify host cellular factors that interact with PV-$2C^{ATPase}$.

**FUTURE DIRECTIONS**

I generated a PV $2C^{ATPase}$ three-dimensional structure and a putative hexamer model. I have provided validation of the three-dimensional structure by positively identifying an insertion tag site. However, further studies of the putative oligomeric state of $2C^{ATPase}$ are required. The putative hexamer revealed two charged amino acids ($K_{168}$ and $R_{226}$) (FIGURE 8) that form the core of the hexamer. Mutating the core amino acids will provide insight detail into the putative function of the protein. PV $2C^{ATPase}$ is often treated and described as a monomer, however it is not clear whether its also functions in the oligomeric state. Recent studies have implicated $2C^{ATPase}$ as being a helicase or RNA destabilizer, and the removal of the N-terminal region resulted in the loss of ATPase activity (Adams et al., 2009). It would be interesting to investigate the roles of the hexameric core amino acid in viral replication. Interestingly, the core has two amino acids, $K_{168}$ – facing the N-terminal and $R_{226}$ – facing the C-terminal, that may perform different functions. I recommended a mutational analysis of the charged amino acids to investigate their roles in the viral life cycle.

I also developed mutant viruses that have tag epitopes, and are recognized by their respective antibodies (FIGURE 12 and 13). These PV $2C^{ATPase}$ tagged mutants are very important because they can be used to study the mechanism of viral assembly, in which $2C^{ATPase}$ plays a critical role. Furthermore, PV $2C^{ATPase}$ is known for its multi-functionality and has been implicated in various stages in the life cycle, which suggests that the protein may interact with other proteins for such functions. EV-71 $2C^{ATPase}$ interacts with cellular protein reticulon 3 for viral replication (Tang et al., 2007). The findings in this dissertation lay the foundation for the identification of other host cellular

proteins that PV $2C^{ATPase}$ interacts with for its many functions. I suggest using the tagged viruses to perform a proteomic screen for proteins that interact with $2C^{ATPase}$. The identification of cellular host proteins contributing to the many functions of $2C^{ATPase}$ would be a major advance to the field because it would provide new insights into $2C^{ATPase}$ function with cellular proteins to target as treatment options.

**FIGURE 6. Phyre2 predicted model of the PV 2C$^{ATPase}$ three-dimensional structure.**

(a) The amino acid sequence of PV1(M) was submitted to the Phyre2 online server to generate a 3D structural model (Materials and Methods). The server predicted a 2C$^{ATPase}$ model for 92% of the residues with greater than 90% confidence in the model. The structure of the N-terminal domain, highlighted in black, is highly unreliable. Sequences highlighted in gold are predicted with good confidence. The 2C$^{ATPase}$ structure shown in light green is predicted with 100% confidence. (b) The predicted three domains in the 2C$^{ATPase}$ structure. The N-terminal domain (red) consists of helical structures, the central helicase domain (blue) contains the NTP binding/helicase boxes of A, B and C, and the C-terminal domain (green) consists mostly of helical structures. The flexible region between the central and C-terminal domain contains the $N_{252}$ VP3 capsid interacting residue.

**(a)**

**(b)**
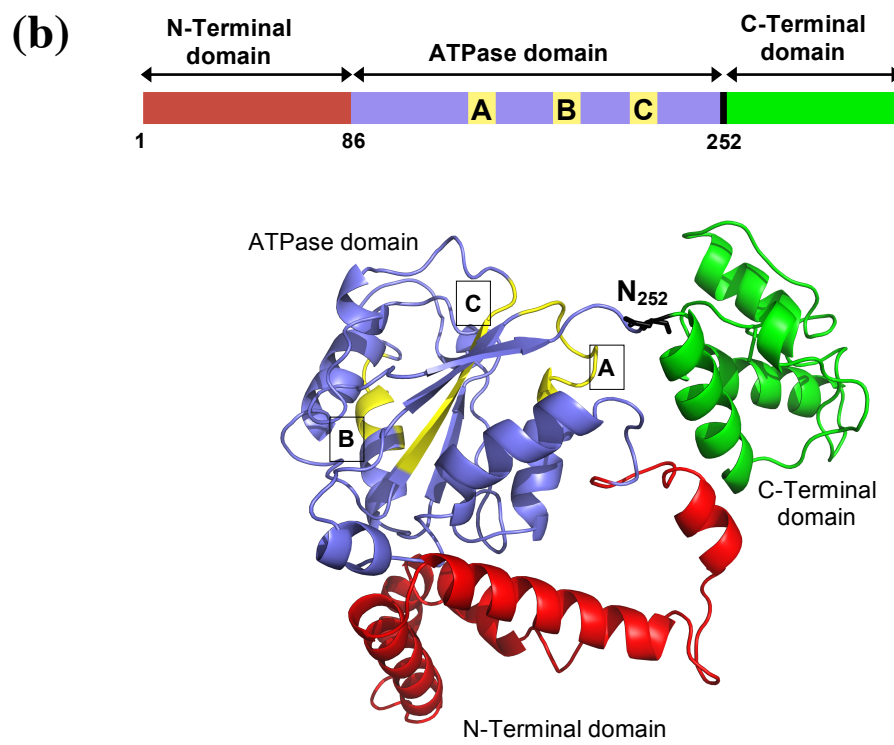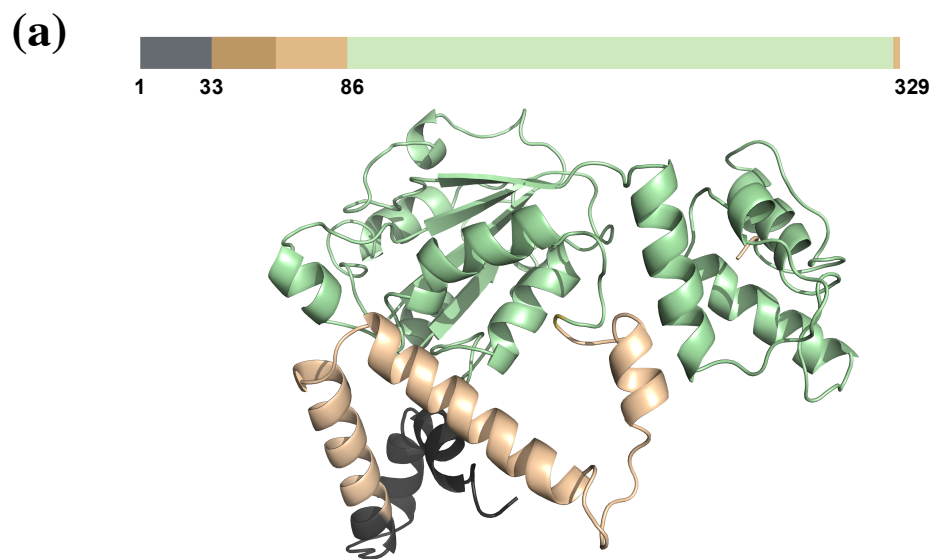
**FIGURE 7. The electrostatic representation of PV 2C$^{ATPase}$ model structure.**
Cartoon models of PV 2C$^{ATPase}$ (gray) is shown in the right panel, and the left panel shows the electrostatic representation of PV 2C$^{ATPase}$. Bottom models are 180$^{o}$ rotations of the top structure on the horizontal axis.

Cartoon representation          Electrostatic representation
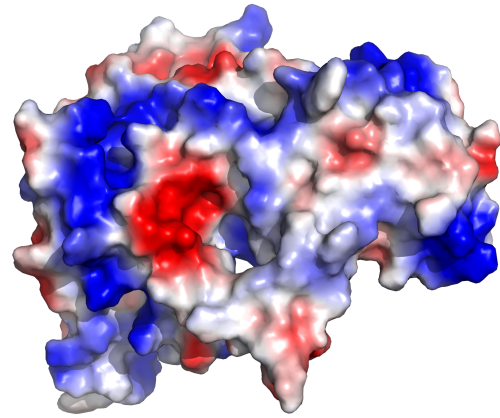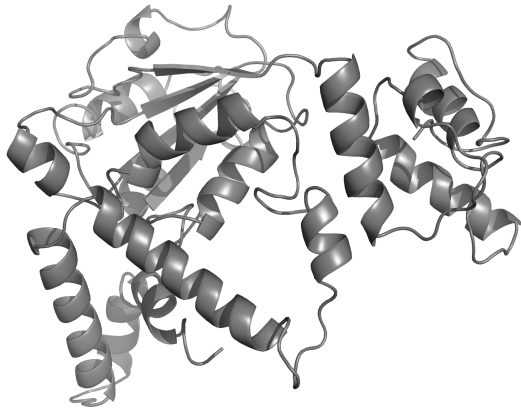


180°
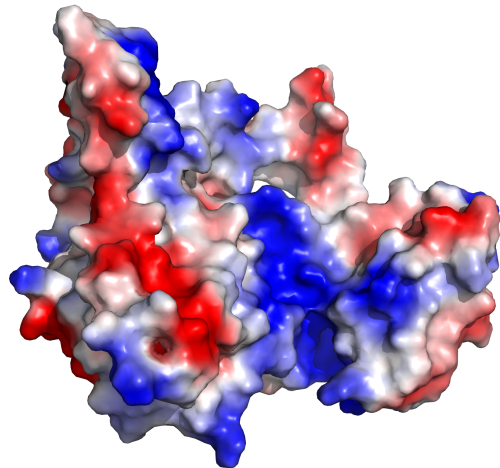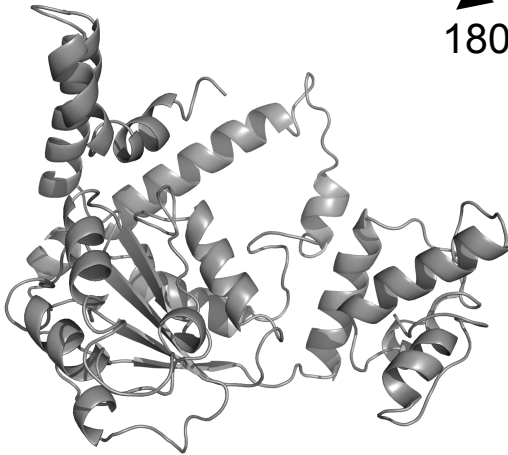
**FIGURE 8. The electrostatic model of the putative 2C$^{ATPase}$ hexamer.** Putative 2C$^{ATPase}$ hexamer was generated by super-positioning the predicted 2C$^{ATPase}$ model to recA (pdb:2rec). (a) Electrostatic representation showing the charges of the putative 2C$^{ATPase}$ hexamer. Displayed residues are primarily composed of the N-terminal amino acids. The core of the hexamer is composed of positively charged amino acids (K$_{168}$ and R$_{226}$), shown on the top right panel. (b) Electrostatic representation of the putative 2C$^{ATPase}$ hexameric model, displaying the C-terminal view. (c) Side view of the putative PV 2C$^{ATPase}$ hexameric model. Blue represents positively charged surfaces and red the negatively charged surfaces.

**(a)** N-terminal view

K168  R226

**(b)** C-terminal view

**(c)** Side view

−74.376    74.376
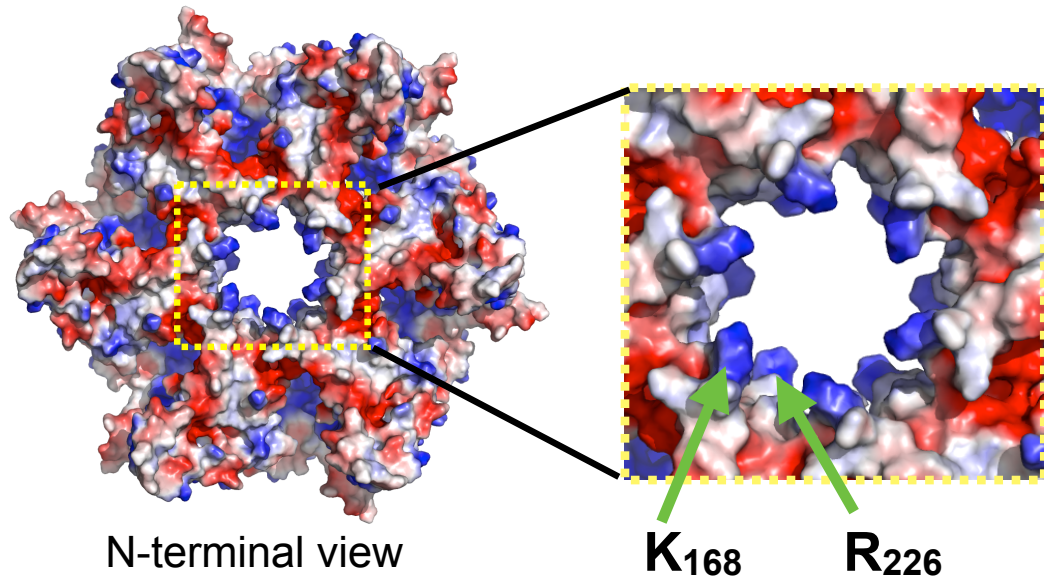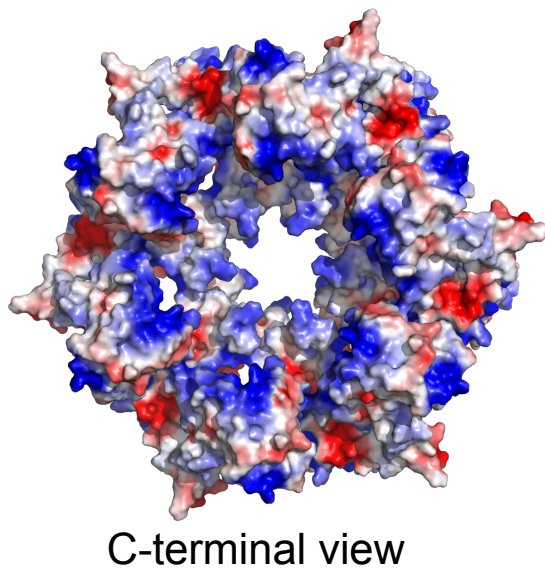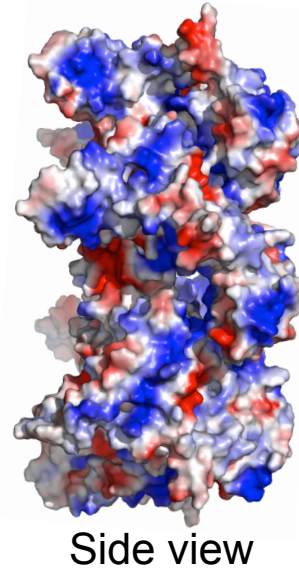
**FIGURE 9. Identification of small tag epitope insertion sites in PV 2C^ATPase.**

Schematic map of 2C^ATPase protein noting the amphipathic helices, and the cysteine-rich

zinc binding region. The two predicted insertion sites are highlighted in orange.

Amino acids in the unstructured sites are in orange and the surrounding helices are in

green. The identified potential sites that may potentially tolerate insertion of small

peptides are shown in orange in the 2C^ATPase confidence model, and are labeled sites I and

II, respectively. The lysine ($K_{270}$), represented in the stick (blue), was incorporated into

the inserted tag (strepII and FLAG) peptides.

Site I    AMATEMCKNCHQPANF
          263                      278

Site II   DKSSRVRYSIDQITTM
          294                      309

**FIGURE 10. Growth and plaque phenotypes of 2C-tag inserted virus mutants.** (a)
Plaque phenotypes of wt-PV1(M), 2C-strepII PV1(M), and 2C-FLAG PV1(M) viruses.
Plaque assays were performed on HeLa cells and incubated for two days. (b) Growth
curve of wt and 2C-strepII mutant viruses. HeLa cells were infected at an m.o.i. of 5 and
incubated at $37^{\circ}$C at various time-points. Recovered viruses from the time-pointe were
titered by plaque assay. Blues line represents wt-PV1(M) and the red line represents 2C-
strepII PV1(M). Subscript under the plaque picture indicates the virus dilution at which
the image was taken.

**(a)**



PV1(M)-wt      PV1(M)-2C-strepII tag      PV1(M)-2C-flag tag
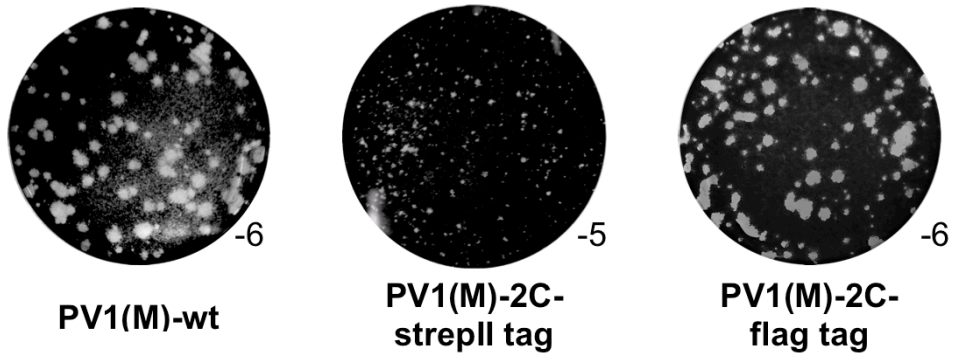
**(b)**
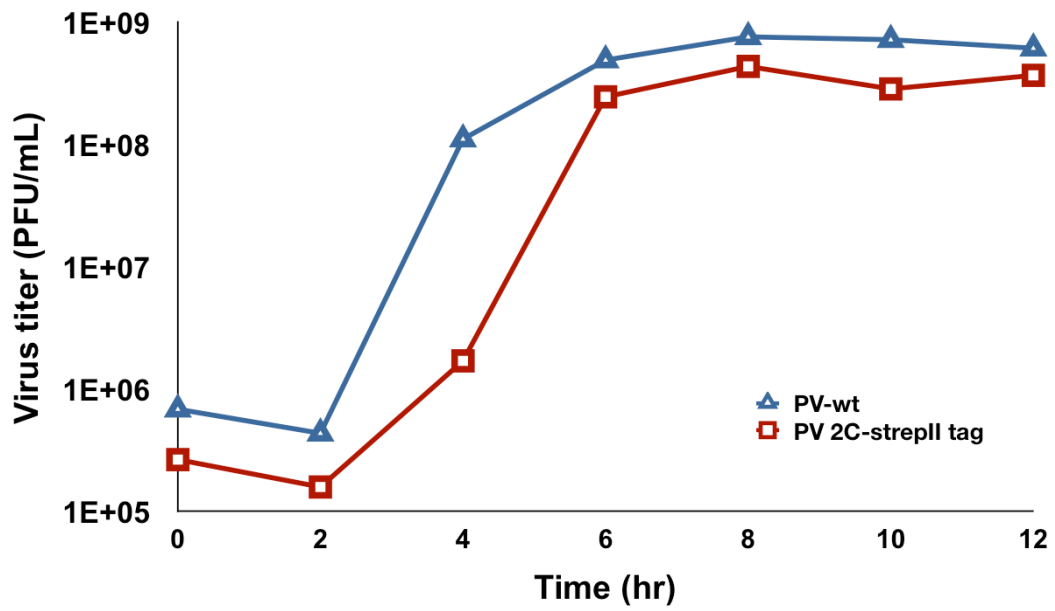
**FIGURE 11. Locations of suppressor mutations in 2C$^{ATPase}$ tag inserted viruses.**
The mutational-map of recovered PV 2C$^{ATPase}$ epitope tagged viruses is shown in a schematic map of non-structural protein 2BC. Locations of suppressors mutations in 2C$^{ATPase}$ or 2B are indicated by red arrow. The original amino acids are separated from the respective suppressor amino acids by the residue position number (in sub-scripted). Below the position amino acids and the corresponding codons for the respective amino acid are shown The bold and capitalized nucleotides represent the suppressor change in the recovered viruses. The right panel shows the passage number where full CPE was observed for the tagged viruses.
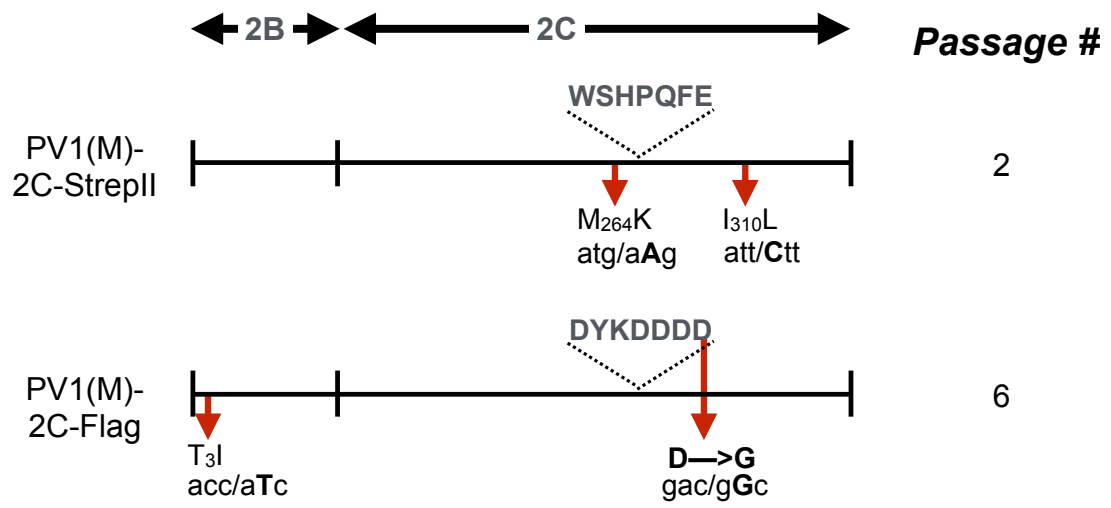
**FIGURE 12. Recognition of tag epitopes in PV 2C$^{ATPase}$ tagged mutants.** HeLa cells were independently infected with wt PV1(M), 2C-strepII PV1(M), and 2C-FLAG PV1(M) viruses at an m.o.i of 10 for 4 hr for wt, and 6 hr for 2C$^{ATPase}$ tag-inserted viruses, respectively. SDS-page/Western analysis was used to detect 2C$^{ATPase}$ proteins in infected HeLa cell lysates. 2C$^{ATPase}$ proteins were detected with antibody against 2C$^{ATPase}$ and the respective tag epitope antibodies. The top panel shows detection of 2C$^{ATPase}$ and its precursor proteins using mouse antibody that recognizes 2C$^{ATPase}$ (red). Rabbit antibody against the strepII epitope was used to detect the strepII tag on the same lysate (shown in green), and a merge that shows the overlap of 2C$^{ATPase}$ and precursors with strepII tag in yellow. The bottom panel shows detection of FLAG epitope of the same lysates but separate SDS-page/western analysis, with mouse antibody against the FLAG epitope.
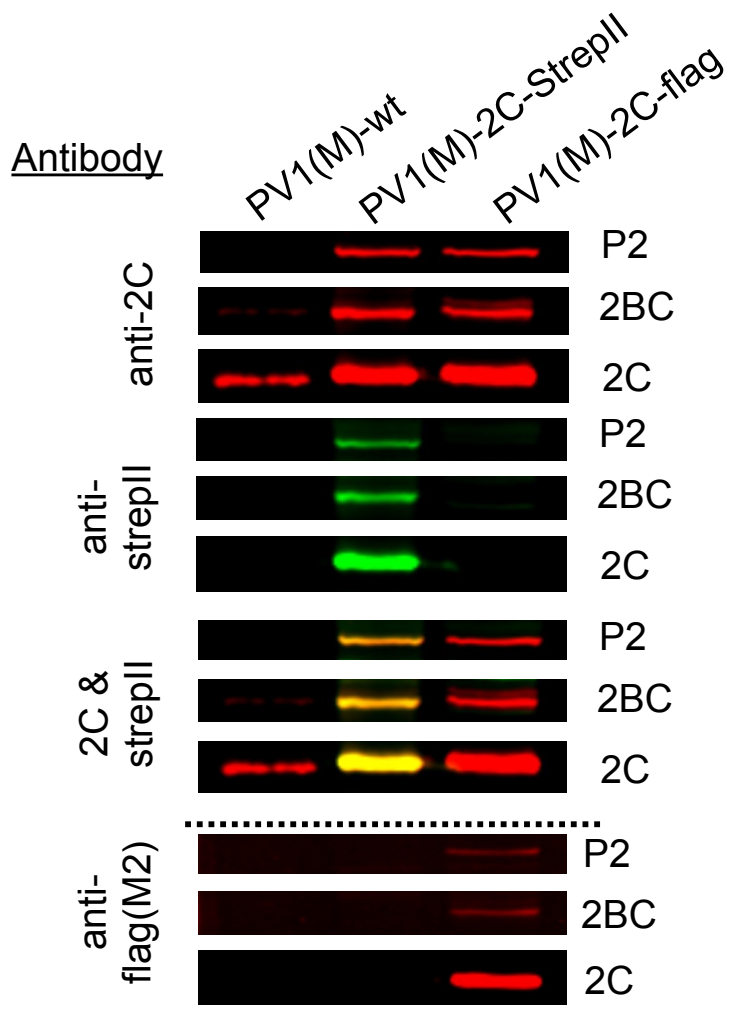
**FIGURE 13. Immunofluorescence imaging of PV 2C-FLAG tag mutant virus in HeLa cells.** HeLa cells were infected at an m.o.i. of 5 and incubated for 4 hr at $37^{\circ}$C. Cells were fixed with paraformaldehyde. Fixed cells were then probed with primary antibodies against FLAG tag epitope and PV1, then followed by alexa fluor 488 (green) and 555 (red) conjugated antibodies, respectively. The cell nucleus was stained with DAPI, shown in blue.

PVI (r)

Flag tag (m)

Merge

Red - PVI
Green - Flag Tag (2C)
Blue - Dapi
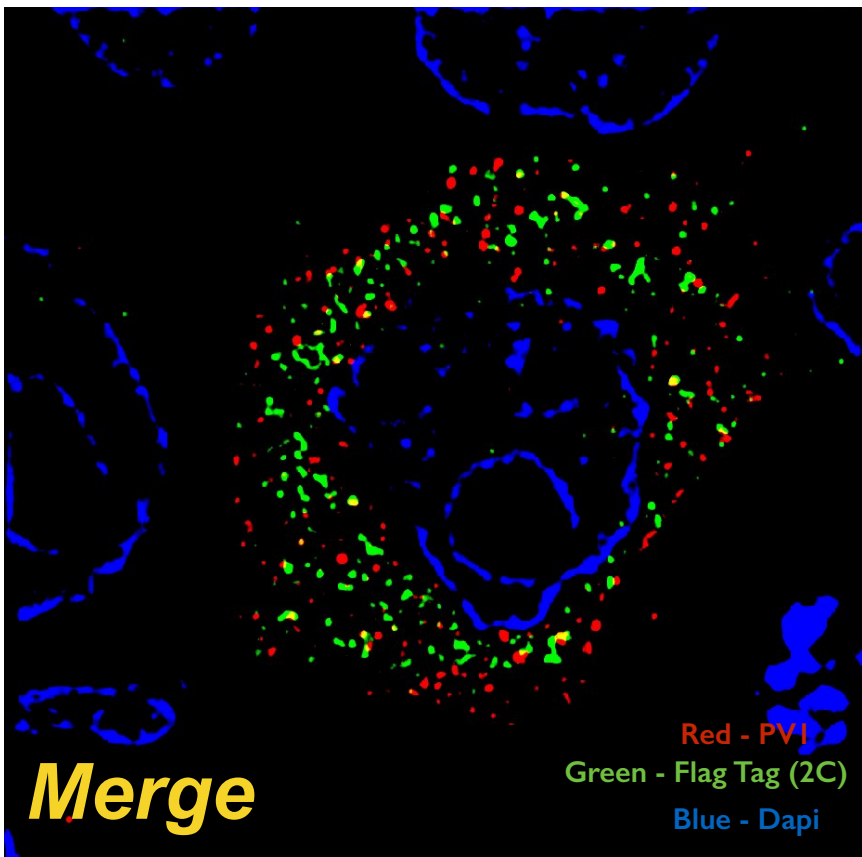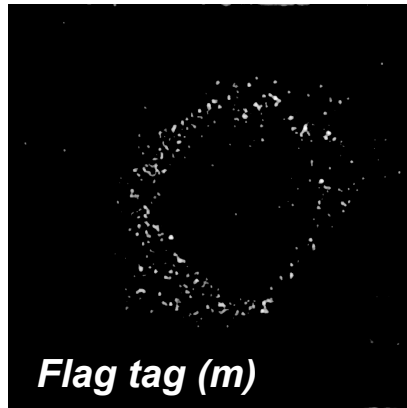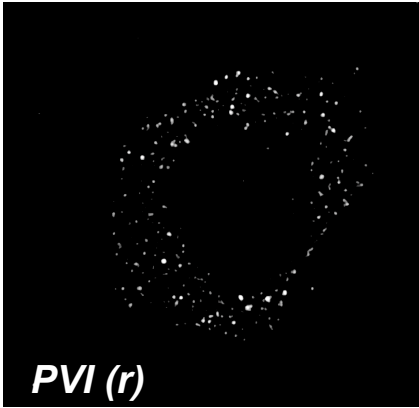
**Table 1**: Summary of the growth phenotypes of triple alanine mutants surrounding $N_{252}$, a capsid interacting site in poliovirus $2C^{ATPase}$.

| Mutants | Mutations in $2C^{ATPase}$. | Time of full CPE and growth phenotype. | | |
|---------|------------------------------|-------------|-------------|-------------|
| | | 33°C | 37°C | 39.5°C |
| FMI/AAA | $F_{244}A/M_{246}A/I_{248}A$ | - | - | - |
| QVM/AAA | $Q_{249}A/V_{250}A/M_{251}A$ | Tf (*q.i.*, ts) | Tf (*q.i.*, ts) | P2 (ts) |
| EYS/AAA | $E_{253}A/Y_{254}A/S_{255}A$ | Tf (ts) | P2 (ts) | - |
| GKL/AAA | $G_{258}A/K_{259}A/L_{260}A$ | - | - | - |

*ts* - temperature sensitive; *q.i.* - quasi infectious

**Chapter 2: Genetics studies of residues near a presumed capsid interacting site in poliovirus protein 2C$^{\text{ATPase}}$**

**RESULTS**

I. Construction of triple alanine mutants and their growth phenotypes

Studies of the role of 2C$^{\text{ATPase}}$ in encapsidation have been hindered by the multifunctional nature of the protein (Wang et al., 2012) as well as by the stringent dependence *in cis* of translation>RNA replication>assembly (Paul and Wimmer, 2015; Wang et al., 2012). Since 2C$^{\text{ATPase}}$ plays an essential role in RNA replication, a step prior to particle assembly, mutations in 2C$^{\text{ATPase}}$ leading to RNA replication defects will also prevent proper encapsidation. Our previous genetic studies with a PV/CAV20 chimera indicated an interaction of N$_{252}$ in PV protein 2C$^{\text{ATPase}}$ with capsid protein VP3 of CAV20 that is required for encapsidation (Liu et al., 2010). Unexpectedly, in the context of the PV polyprotein, N$_{252}$, which falls into a flexible domain of the polypeptide containing unconserved amino acids, (FIGURE 6b, FIGURE 14), is not important for encapsidation. That is, the replacement of N$_{252}$ in PV 2C$^{\text{ATPase}}$ with A, G, S, D, or G had no effect on virus growth (data not shown). We speculate that in the PV background one or more residues in the vicinity of N$_{252}$, in or near the flexible domain, might have a similar function in encapsidation. In this study, I used alanine mutagenesis of selected residues to try to answer this question.

Our laboratory previously performed an alanine screen of all clustered charged residues in 2C$^{\text{ATPase}}$, and we identified further evidence of the 2C$^{\text{ATPase}}$ interaction with capsid protein, and in replication (Wang et al., 2012). I focused on a flexible region near N$_{252}$ in this study. I selected triple hydrophobic amino acids or single charged residues

near $N_{252}$ that had not been previously analyzed. First, I designed and constructed four triple alanine mutants, two upstream [$F_{244}A/M_{246}A/I_{248}A$ (FMI/AAA) and $Q_{249}A/V_{250}A/M_{251}A$ (QVM/AAA)] and two downstream [$E_{253}A/Y_{254}A/S_{255}A$ (EYS/AAA) and $G_{258}A/K_{259}A/L_{260}A$ (GKL/AAA)] of $N_{252}$, respectively (Table 2; FIGURE 14).

To compare the growth phenotypes of the triple alanine mutants with that of the wt virus, I transfected RNA transcripts into HeLa R19 cells. The transfected cells were incubated either at $33^{o}C$, $37^{o}C$ or $39.5^{o}C$ for approximately 72 hr or until full cytophathic effect (CPE) developed. Two constructs (FMI/AAA and GKL/AAA) produced no progeny even after 10 passages on fresh HeLa cells at all temperatures tested (Table 2, FIGURE 15a). One mutant (EYS/AAA) exhibited wt-like growth at $33^{o}C$ but at $37^{o}C$ progeny was produced only after two passages on fresh HeLa cells (Table 2, FIGURE 15a). The second viable mutant, (QVM/AAA), was defective in growth at $39.5^{o}C$ but produced progeny at $33^{o}C$ or $37^{o}C$ (Table 2, FIGURE 15 a and b). Lysates of the two viable viruses, obtained from $33^{o}C$ transfections, were titered by plaque assays at $33^{o}C$, $37^{o}C$ or $39.5^{o}C$. As shown on FIGURE 15b, virus titers at $37^{o}C$ and at $39.5^{o}C$ were significantly lower with both mutants than what was obtained with the wt virus. The QVM/AVA variant and the EYS/AAA virus exhibited mostly tiny plaques at all temperatures tested (FIGURE 15c).

Viral RNAs were extracted from lysates of the two viable triple alanine mutants, grown at different temperatures, and were subjected to RT/PCR and full length genome sequencing. The results indicated that QVM/AAA is quasi-infectious thus progeny viruses isolated from HeLa cell lysates were always found to be genetic variants of the

68

input sequence (Gmyl et al., 1993). It produced a variant with a single nucleotide reversion QVM/AVA while no nucleotide substitutions were observed with the EYS/AAA mutant (FIGURE 15a).

II. Triple alanine *ts* mutants are defective in RNA replication at 39.5$^{\mathrm{o}}$C

The two *ts* triple mutants, EYS/AAA and the partial revertant of QVM/AAA (QVM/AVA) that grew poorly at 39.5$^{\mathrm{o}}$C were further analyzed to test for any defects in RNA replication. Viruses grown at 33$^{\mathrm{o}}$C were used to infect HeLa cells at 39.5$^{\mathrm{o}}$C and aliquots were taken at various times post-infection. RNA levels in lysates of cells infected with these viruses were measured by qPCR. Both mutants exhibited a severe defect in RNA replication at 39.5$^{\mathrm{o}}$C when compared to the wt virus (FIGURE 16). Since encapsidation is dependent upon normal RNA replication, these mutants were not further analyzed for any additional encapsidation defects.

III. Nonviable triple alanine mutants exhibit normal protein synthesis and processing

To rule out the possibility that the lethal growth phenotypes of the FMI/AAA and GKL/AAA mutants were due to a defect in protein translation or polyprotein processing, I translated RNA transcripts of these mutants in HeLa cell free extracts. After incubation for 8 hrs at 34$^{\mathrm{o}}$C, the samples were analyzed by SDS-polyacrylamide gel electrophoresis. As shown on FIGURE 17, both mutants exhibited normal protein synthesis and polyprotein processing profiles. Surprisingly, the amino acid substitutions with alanine did not influence the migration of the 2C$^{\mathrm{ATPase}}$-related polypeptides when compared to wt translations patterns, as observed in the previous clustered alanine scanning study (Wang et al., 2012).

IV. Construction and growth properties of single alanine mutants

Triple alanine mutants that displayed a lethal growth phenotype (FMI/AAA, GKL/AAA) were subsequently scanned by single alanine mutagenesis to identify the specific residues responsible for the growth defect. Of the amino acids contained within FMI and GKL, five ($F_{244}A$, $M_{246}A$, $I_{248}A$, $K_{259}A$, $L_{260}A$) were mutated to alanine (FIGURE 18, Table 3). RNA transcripts of the five-alanine mutant cDNAs were transfected into HeLa cells at $37^{o}C$ and their growth phenotypes were examined. The $F_{244}A$ mutant was not viable and did not produce any progeny even after several passages on HeLa cells. The lethal growth phenotype was not due to a defect in translation or protein processing as shown by *in vitro* translation of mutant RNA transcripts in HeLa cell free extracts (FIGURE 19a). However, qPCR analysis of viral RNA levels in infected cells indicated a defect in RNA replication (FIGURE 19b) and therefore the mutant was not further analyzed for an encapsidation defect.

Two of the mutants ($I_{248}A$, $L_{260}A$) were quasi-infectious and produced ($A\rightarrow V$) variants during transfection or first passage indicating that the original alanine residues at these positions were nonfunctional (FIGURE 18; Table 3). Although the $M_{246}A$ virus was viable it quickly mutated to a V, yielding a $M_{246}V$ variant. Viruses derived from $37^{o}C$ transfections were plaque titered at $33^{o}C$, $37^{o}C$ and $39.5^{o}C$ (FIGURE 18b). The $I_{248}V$ variant was *ts* with a particularly strong growth defect at $39.5^{o}C$ but less prominent at $33^{o}C$ or $37^{o}C$. The $M_{246}V$ variant exhibited a mildly lower titer than the wt at all three temperatures tested while the $L_{260}V$ variant grew nearly as well as the wt virus. The plaque sizes of the single alanine mutants or the valine variants were somewhat smaller at $37^{o}C$ or $39.5^{o}C$ than that of the wt (FIGURE 18c).

The last of the single mutants, $K_{259}A$, produced progeny during transfection, and my preliminary studies indicated that it was cold sensitive and retained its original alanine mutation genotype even after several passages at 33$^o$C (FIGURE 18 a and b). It should be noted that of other cold sensitive mutants of poliovirus known thus far, one was shown to be defective in uncoating due to a possibly defect in virion structure (Li and Baltimore, 1990), and the other had a mutation in the viral protein 3A that impairs viral RNA synthesis (Berstein and Baltimore, 1988). The uncoating cold sensitive $2C^{ATPase}$ mutant contained a linker insertion (4 amino acids) between residues 255 and 256, just upstream of $K_{259}$, and two secondary mutations at $M_{293}V/R_{295}K$ that were obtained after passaging at 39.5$^o$C (Li and Baltimore, 1990). Interestingly, a single $N_{140}S$ change was able to suppress the cold sensitive growth phenotype, suggesting an interaction between the C-terminal domain of the polypeptide and a domain between boxes A and B of the NTP binding domain (Li and Baltimore, 1990). We have similarly postulated an interaction between these domains from our previous alanine scanning analyses (Wang et al., 2014; 2012). Based on these previous studies, our $K_{259}A$ mutant appeared to be a good candidate in the search of a possible encapsidation/uncoating defect.

V. $2C^{ATPase}$ $K_{259}A$ mutant exhibits a delay in growth and protein synthesis at 35$^o$C and 33$^o$C

To learn more about the cold sensitive phenotype of this mutant, viruses grown at 37$^o$C were used to infect HeLa cells (m.o.i. 5) at 37$^o$C, 35$^o$C or 33$^o$C. When compared to the wt virus, the cold sensitive mutant exhibited increasingly longer delays in growth when the temperature of the infection was reduced from 37$^o$C to 35$^o$C and then to 33$^o$C, respectively (FIGURE 20a). The replication of $K_{259}A$ mutant virus reached wt levels at

10 and 6 hr post-infection, respectively, in comprising to wt virus at 33$^o$Cand 37$^o$C

(FIGURE 20a). These results suggested a defect at an early step of infection with the

K$_{259}$A virus, possibly in uncoating.

Protein synthesis immediately follows uncoating in the viral life cycle, I reasoned

that the K$_{259}$A mutant might also exhibit a delay in protein synthesis at 33$^o$C and at 35$^o$C

when compared to the wt virus. Virus stocks generated at 37$^o$C was used to infect HeLa

cells at different temperatures at an m.o.i. of 5 (FIGURE 20b). At various times post

infection lysates were analyzed on SDS-polyacrylamide gels and the 2C$^{ATPase}$-related

proteins were identified by Western analysis using an antibody to 2C$^{ATPase}$. Relative to

the wt virus, there was a small delay in protein synthesis by the mutant at 37$^o$C and

increasingly longer delays when the temperature was reduced from 37$^o$C to 35$^o$C and

33$^o$C, respectively (FIGURE 20b). The results parallel the growth kinetics of the mutant

virus at 33$^o$C, 35$^o$C and 37$^o$C when compared to the wt virus and provide further

evidence that the cold sensitive mutant is defective in uncoating at the restrictive

temperatures.

V. The 2C$^{ATPase}$ K$_{259}$A mutant is defective in encapsidation at 33$^o$C and 35$^o$C

The delayed growth and protein synthesis by the K$_{259}$A mutant at 33$^o$C suggested

the possibility of a defect at some stage of uncoating. However, since 2C$^{ATPase}$ is not a

part of the virus particle and is synthesized after viral entry and uncoating, a direct role

for this protein in this process can be ruled out. To decipher the mechanism by which a

mutation in 2C$^{ATPase}$ might affect uncoating, I tested for defects in RNA replication and

encapsidation using an R-Luc reporter virus (FIGURE 21). In this construct, R-Luc is

fused to the N-terminus of the PV polyprotein (Liu et al., 2010). After infection, the

chimera synthesizes the polyprotein from which the N-terminus of the R-Luc reporter protein is cleaved by 3CD$^{pro}$ after which it signals the extent of protein translation and RNA replication (Liu et al., 2010). I used T7 RNA transcripts of the chimeric virus constructs (wt and K$_{259}$A mutant) and transfected these into HeLa R19 cells at different temperatures in the absence and presence of guanidine hydrochloride (GnHCl), a potent inhibitor of PV RNA replication (Pincus et al., 1986). Luciferase activity was measured 16 hr post-transfection. In the presence of GnHCl the R-Luc activity measures translation of the input RNA while in the absence of the drug the R-Luc signal represents both translation and RNA replication. To measure encapsidation, cell lysates from transfections made in the absence of GnHCl, were then passaged to fresh HeLa cells and R-Luc activity was measured 8 hr post-infection. The results indicate that at 37$^{o}$C, both RNA replication and encapsidation of the K$_{259}$A mutant nearly matched the level observed with the wt construct (FIGURE 21). At 35$^{o}$C, passaging to new HeLa cells reduced the R-Luc signal for both the wt and mutant constructs although the decrease was more pronounced with the mutant, an observation suggesting a small encapsidation defect relative to the wt. However, at 33$^{o}$C the mutant exhibited a small (~ 2 fold) reduction in RNA replication, but a striking 25-fold decrease in R-Luc signal that measures encapsidation. It is unlikely that such a small decrease in RNA replication would result in a very large defect in encapsidation. I infer that the K$_{259}$A mutant is severely defective in encapsidation at 33$^{o}$C. In view of these results it would be to also test the effect of the encapsidation defect on uncoating with virus grown at 33$^{o}$C. Unfortunately, we were not able test this because of the very low titer of the mutant virus in cells grown under these conditions (FIGURE 18b).

VI. Immunofluorescence imaging shows inhibition of mature virus production with the

K$_{259}$A mutant at 33$^{\text{o}}$C

The inhibition of encapsidation, resulting in decreased amounts of infectious virus at 33$^{\text{o}}$C (FIGURE 22), was confirmed by immunofluorescence imaging. K$_{259}$A virus, grown at 37$^{\text{o}}$C, was used to infect HeLa cells at 37$^{\text{o}}$C, 35$^{\text{o}}$C and 33$^{\text{o}}$C at an m.o.i. of 5 and incubation continued for 4 hrs, 5 hrs and 6 hrs, respectively, at the same temperatures. Infected lysates were probed with monoclonal antibodies to 2C$^{\text{ATPase}}$ and A12 antibodies, the latter recognizing mature virus (Chen et al., 2013). As shown in Fig.7, both the localization and quantity of mature virus is comparable with the two viruses at 37$^{\text{o}}$C and 35$^{\text{o}}$C. However, at 33$^{\text{o}}$C there is a strong reduction in the amount of mature virus present in K$_{259}$A-infected cells when compared to the wt virus. In addition, there are differences in the localization of 2C$^{\text{ATPase}}$ in the wt and mutant virus-infected cells. In wt virus-infected cells, 2C$^{\text{ATPase}}$ localizes in the perinuclear region of the cell while this protein is primarily in the cytoplasm of all infected with the mutant. Taken together our results clearly indicate a relationship between the encapsidation defect of the K$_{259}$A mutant at 33$^{\text{o}}$C, the production of mature virus, and a delay in uncoating and protein synthesis during the next cycle of virus growth.

**DISCUSSION**

The aim of these genetic studies was to search for and identify one or more sites in protein $2C^{ATPase}$ near $N_{252}$, a residue identified to be essential in the assembly of a PV/CAV20 chimera (Liu et al., 2010). $N_{252}$ maps to a variable flexible region within $2C^{ATPase}$ (FIGURE 6b, FIGURE 15 a and b), a site presumed suitable for an interaction between the viral ATPase and a capsid polypeptide. It should be noted, however, that the asparagine at position 252 of PV $2C^{ATPase}$ is not conserved amongst enteroviruses, not even among the three poliovirus serotypes or CAV20, and is the direct capsid interacting site of the PV/CAV20 chimera. Thus, I speculated, that there are residues in the variable flexible region other than $N_{252}$, or in addition to $N_{252}$, which play a role as the presumed capsid interacting site involved in particle assembly.

Encapsidation is the last step in the viral replicative cycle providing to newly synthesized genomes a protective protein coat that, in turn, is required for a virion's attachment to and penetration into a new host cell. Attachment and penetration leads to uncoating of the genome, a complex process involving structural alterations to the viral capsid and release of the infectious genomic RNA into the cytoplasm. Uncoating and encapsidation are linked since the normal release of the genome depends upon correctly assembled virion particles (Hogle, 2002). With poliovirus, uncoating begins with the loss of VP4 from the capsid, followed by the loss of VP2, and finally the dissociation of VP1/VP3 and the viral RNA (De Sena and Torian, 1980; Fenwick and Wall, 1973; F. Koch and G. Koch, 1985; Lonberg-Holm et al., 1975).

Drug inhibition (Vance et al., 1997) and genetic experiments (Liu et al., 2010; Wang et al., 2014; 2012) have led to the surprising observation that $2C^{ATPase}$ was not only

essential in genome replication, but also in virion assembly (Jiang et al., 2014). More surprising was that an RNA packaging signal is not involved in poliovirus assembly (Jiang et al., 2014) rather $2C^{ATPase}$ interacts with capsid proteins thereby providing assembly specificity. Moreover, mutations influencing PV assembly seemed to map over a wide range of the $2C^{ATPase}$ polypeptide. Apart from studies with hydantoin (Vance et al., 1997) or with the enterovirus chimera (Liu et al., 2010), alanine scanning mutagenesis of $2C^{ATPase}$ indicated that residues $K_{279}/R_{280}$ and $C_{272}/H_{273}$ within the C-terminal $Zn^{++}$ binding domain (Wang et al., 2012) (residues 269-286) are involved in encapsidation and/or uncoating (Pfister et al., 2000; Wang et al., 2014; 2012). A report of the involvement of $2C^{ATPAse}$ in uncoating, deduced from suppressor mutations ($M_{293}V/K_{295}R$) near a linker insertion (Li and Baltimore, 1990) was particularly interesting. Suppressor variants of the $K_{279}A/R_{280}A$ mutant indicated that this site interacts both with capsid proteins VP1 and VP3, possibly in the context of one or more capsid precursors or the fully assembled capsid (Wang et al., 2012). On the other hand, suppressor variants of the $C_{272}A/H_{273}A$ revealed an interaction with an upstream segment of the $2C^{ATPase}$ polypeptide located between boxes A and B of the NTP binding domain (Wang et al., 2014; 2012).

In the current studies I have first introduced triple alanine mutations into PV protein $2C^{ATPase}$, near $N_{252}$ (Figs. 2b-d), with the aim of searching for additional sites near the C-terminus of the polypeptide that are required for encapsidation. We selected mutants for analysis that fell either into highly structured or flexible domains. We identified two triple alanine mutants (FMI/AAA and GKL/AAA) that possessed lethal growth phenotypes at all temperatures tested ($33^{o}C$, $37^{o}C$, $39.5^{o}C$). These mutations are

predicted to be located in a β sheet and an α helical domain, respectively of the $2C^{ATPase}$ structural model. In addition, we observed two mutants that were *ts* and/or quasi-infectious, exhibited normal protein translation and processing profiles, but were defective in RNA replication (EYS/AAA and QVM/AAA). These mutations fell into a partly or fully flexible stretch of residues in the predicted $2C^{ATPase}$ structure. Since the processes of encapsidation and RNA replication are linked we cannot exclude the possibility that these mutants also had encapsidation defects, independent of RNA replication. It should be noted that an $E_{253}G$ change in PV $2C^{ATPase}$ was previously shown to yield a small plaque virus, to prevent secretion inhibition in tissue culture cells (Burgon et al., 2009) and to produce a VCP-knockdown resistant PV mutant (Arita et al., 2012). Whether the $E_{253}A$ substitution, within the context of the EYS mutation, would cause similar defects is not known.

To identify the specific residues responsible for the lethal growth phenotypes of the triple alanine mutants we scanned them by single alanine mutagenesis. The mutants included $F_{244}A$, $I_{248}A$, $K_{259}A$, and $L_{260}A$, residues that are highly conserved in picornavirus $2C^{ATPase}$ proteins and $M_{246}$, which is less conserved (FIGURE 14c). Mutant $F_{244}A$ was nonviable and had a severe defect in RNA replication (FIGURE 19). Interestingly, our previous alanine mutagenesis of positively charged residues $R_{240}/R_{241}$ and $D_{245}/D_{247}$, in close vicinity of $F_{244}$, also resulted in lethal growth phenotypes and severe replication defects (Wang et al., 2012). Three of the single alanine mutants ($M_{246}A$, $I_{248}A$ and $L_{260}A$) were quasi-infectious and produced variants that had either wt or *ts* growth phenotypes. In all cases ($M_{246}A$, $I_{246}A$, $L_{260}A$), the variants contained an exchange of a moderately hydrophobic residue, alanine, with a more hydrophobic and

77

larger amino acid, valine. The original residues, $M_{246}$, $I_{246}$ and $L_{260}$ are also strongly hydrophobic and larger than the alanines that replaced them. It should also be noted that reversion to the original genotypes would have required two simultaneous nucleotide substitutions while the A→V changes occurred with the replacement of a single nucleotide.

The last single alanine mutant $K_{259}A$ was cold sensitive and exhibited a delay in growth and in protein synthesis at the restrictive temperatures, $35^{\circ}C$, and particularly at $33^{\circ}C$. Our experiment with a reporter virus indicated a specific defect in encapsidation at these temperatures. Interestingly, although this defect was not detectable at $37^{\circ}C$ with this assay, an abnormality in virion structure, presumably resulting from imperfect encapsidation at this temperature, could be inferred from the following observations. Mutant viruses grown at $37^{\circ}C$ were strongly delayed both in growth and in protein synthesis when used for infections and growth at $35^{\circ}C$ or $33^{\circ}C$ (FIGURE 20 a and b). Immunofluorescence imaging of cells infected with the wt and mutant viruses confirmed the nearly total lack of mature virus production by the mutant at $33^{\circ}C$, 6 hr post infection (FIGURE 22). In addition, the imaging experiments revealed differences in the localization of $2C^{ATPase}$ with the wt and the mutant viruses at $33^{\circ}C$. While the wt virus exhibited $2C^{ATPase}$ localization in the perinuclear region of the cell the mutant protein was primarily in the cytoplasm.

The $K_{259}$ residue in poliovirus $2C^{ATPase}$ adds to the previously discovered locations near the C-terminus of the polypeptide that are involved in encapsidation/uncoating. This domain extends from residue $N_{252}$, to the $M_{293}/K_{295}$ suppressor mutations of a linker insertion at residues 255/256 of the cold sensitive mutant of Li and Baltimore (Li and

78

Baltimore, 1990). Within this segment of the polypeptide 4 residues are known to be involved in encapsidation/uncoating ($C_{272}$/$H_{273}$ and $K_{279}$/$R_{280}$) (Wang et al., 2014; 2012). Charged residues in proteins are frequently involved in important protein/protein interactions (Diamond and Kirkegaard, 1994) such as the $2C^{ATPase}$/capsid interactions we have previously discovered with the isolation of suppressor mutants to charged to alanine substitutions of residues required for encapsidation (Wang et al., 2012). Although no suppressor variants were identified with the $K_{259}A$ mutant, since the substitution affects encapsidation/uncoating one might speculate that this residue is also involved in some form of interaction with capsid proteins and/or capsid precursors.

As mentioned above, the asparagine at position 252 is not conserved in an alignment of picornavirus $2C^{ATPase}$ proteins and even in different poliovirus serotypes (Fig. 2e). Not surprisingly, the $N_{252}$ in PV1(M) can be replaced with S, G, A or D without any deleterious effect on viral growth (Liu et al., 2010) (unpublished data). Some residues in the immediate vicinity of $N_{252}$, which were included in our mutational analyses ($M_{246}$, $Q_{249}$, $M_{251}$, $E_{253}$, $S_{255}$), are also poorly conserved (FIGURE 14c). However, we suggest that the growth phenotypes of the mutants correlated with the extent of conservation of amino acids within this domain of the protein. Accordingly, the two mutants with the highest conservation (FMI/AAA, GKL/AAA) exhibited lethal phenotypes while mutants (EYS/AAA and QVM/AAA) that were either *ts* or quasi-infectious, respectively, contained substitutions in the variable region.

$2C^{ATPase}$ is one of the most conserved proteins of enteroviruses. However, the residues surrounding $N_{252}$ in $2C^{ATPase}$ are not conserved at all (FIGURE 14c) (Jiang et al., 2007). We speculate that this variable region in picornavirus $2C^{ATPase}$ polypeptides

(FIGURE 14c) plays a crucial role in assembly through the interaction with capsid proteins. Whereas the capsid proteins may have retained a freedom of variation dictated by the formation of receptor and antibody binding sites, $2C^{ATPase}$, a crucial enzyme in genome replication and a player in the rearrangement of the cytoplasmic environment, was restricted to a small segment in a crucial protein-protein binding event. Interestingly, we did not identify any encapsidation mutants in the variable flexible region and our current and previous data (Liu et al., 2010) indicate that this region is important for RNA replication. However, we cannot rule out the possibility of an additional encapsidation defect with any of the mutants analyzed or a role of this domain in interaction with the capsid. Although $K_{259}$ is located in an adjacent a helix, it is feasible that it has some influence on the variable region in a way to alter its interaction with the capsid (FIGURE 14 a and b).

As was postulated before (Hogle, 2002; Li and Baltimore, 1990; Wang et al., 2014), my data are consistent with a link between assembly and uncoating. My genetic studies reported here identify $K_{259}$ as a residue critical for virion assembly and the subsequent step of uncoating during the next cycle of infection. Although many unanswered questions still exist about the roles of $2C^{ATPase}$ in morphogenesis and uncoating these results together with previous alanine scanning experiments demonstrate the usefulness of genetic analyses with *ts* and quasi-infectious variants for the identification of residues important for these processes.
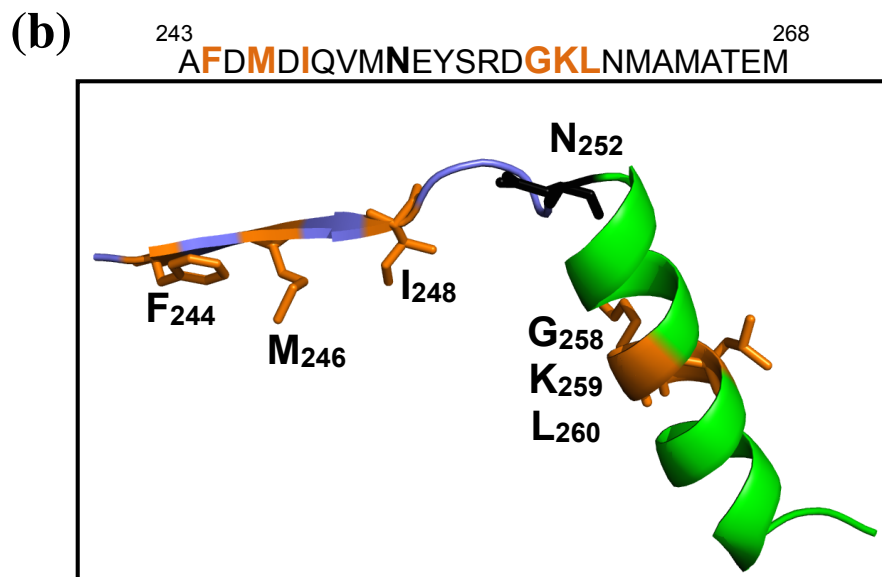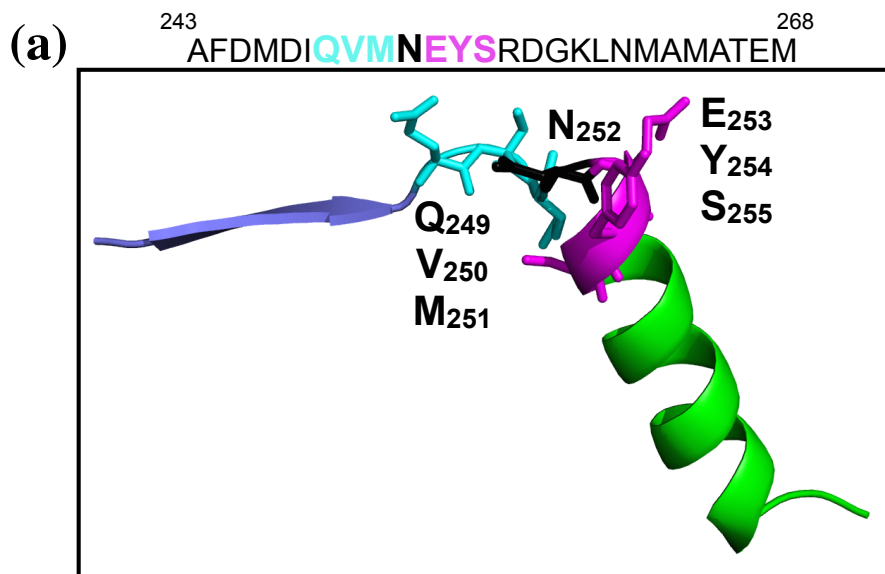
**FUTURE DIRECTIONS**

The $K_{259}A$ *c.s.* mutant virus is an interesting candidate for further investigation of virus morphogenesis. I characterized a mutant that is defective in encapsidation and uncoating. However, I did not show evidence for a specific defect at $33^oC$ or a mechanism. Crystal structure analyses of capsid surface peptides of the mutant would provide useful information on the structure that causes the encapsidation defect, particularly in canyons that are believed to have receptor binding. It seems that $2C^{ATPase}$ functions as a "key" that locks the capsid. There is no evolutionary pressure for the virus to revert to the mutated alanine at $2C^{ATPase}$ position 259. Unfortunately, I did not observe suppressor mutations in any structural protein, which would have provided some insight into the physical interactions of $2C^{ATPase}$ with capsid proteins. The 14S pentamer made by the mutant would also be an interesting target for further investigation. For example does the pentamer exhibit a structural defect? Though $2C^{ATPase}$ is not packaged with the virus, it associates with the 14S particle *in vitro* (Rombaut et al., 1990). In addition, a study of the *c.s.* mutant's ability to form A-particles (135S) would be interesting, which might provide useful insight  into the uncoating defect.

Another interesting experiment would be to change $K_{259}$ to negatively charged amino acids (D or E) rather than to A. This could exacerbate the defect and potentially force the development of suppressor mutations if the *c.s.* defect is charge dependent. Electrostatic representation shows that the $K_{259}$ amino acid localizes to a pocket that is highly positively charged. The $K_{259}A$ *c.s.* defect can be attributed to either a size constraint or the removal  of  the positively change amino acid. A more severe mutation might apply more pressure on the virus, which may force the mutant virus to genetically

compensate and might even develop a suppressor mutation in the capsid, which would indicate a direct protein-protein interaction at the $2C^{ATPase}$ 259 position with the capsid.

Lastly, the Sabin viruses that are used for OPV vaccines are also temperature sensitive, they are sensitive to higher temperatures. The attenuation of the Sabin strains is attributed primarily to few mutations that map to the 5'NTR and capsid regions. The attenuation of Sabin strains' are associated with capsid stability (Macadam et al., 1991). My *c.s.* 2C-K$_{259}$A mutant virus also has a capsid abnormality that should be further investigated *in vivo* both in tissue culture and in mice. It would be very interesting to examine the effect of abnormal encapsidation and uncoating defects on virus attenuation.

**FIGURE 14. The N$_{252}$ residue is located in a flexible region between the ATPase domain and the C-terminal domain.** (a) Locations of the triple alanine mutations on the predicted 2C$^{ATPase}$ structure are illustrated. The QVM residues are in a flexible domain while the EYS residues are partly in a a helical structure. (b) The FMI residues are predicted to be located in a β sheet and the GKL residues are in an α helix structure. (c) Alignment of *Picornavirus* 2C$^{ATPase}$ proteins surrounding residues N$_{252}$. The amino acid sequence of *Picornavirus* 2C$^{ATPase}$ proteins, surrounding N$_{252}$, is shown. Stars indicate the highly conserved residues over a black background and the less conserved residues are shown with a gray background. Dashes indicate the absence of certain residues in the sequences alignment. The size and location of the flexible region are also indicated. The *Enterovirus* 2C$^{ATPase}$ protein are boxed to separate them from the more distantly related picornaviruses (FMDV:*Aphtovirus* genus, EMCV:*Cardiovirus* genus).

**(a)**

<superscript>243</superscript> AFDMDI**QVM****N****EYS**RDGKLNMAMATEM <superscript>268</superscript>



**(b)**

<superscript>243</superscript> A**F**D**M**D**I**QVM**N**EYSRD**GKL**NMAMATEM <superscript>268</superscript>

**(c)**



Flexible Region

|  | ★ ★ | ★ | ★ | | ★ | ★ | | |
|---|---|---|---|---|---|---|---|---|
| **PV1 / 240-270** | RRFAFDMDIQ | VMNEYSR-D- | G-K-LNMAMA | TEMCK |
| **PV2 / 240-270** | RRFAFDMDIQ | IMSEYSR-D- | G-K-LNMAMA | TEMCK |
| **PV3 / 240-270** | RRFAFDMDIQ | VMGEYSR-D- | G-K-LNMAMA | TEMCK |
| **CAV20 / 240-270** | RRFAFDMDIQ | VMGEYSK-D- | G-K-LNMAMA | TEMCK |
| **CVB3 / 240-270** | RRFHFDMNIE | VISMYSQ-N- | G-K-INMPMS | VKTCD |
| **EV71 / 240-271** | RRFYMDCDIE | VTDSYKT-DL | G-R-LDAGRA | AKLCS |
| **HRV2 / 233-264** | RRFFLDLDII | VHDNFKDPQ- | G-K-LNVAAA | FRPCD |
| **HRV14 / 240-270** | RRFGFDLDIC | LHTTYTK-N- | G-K-LNAGMS | TKTCK |
| | | | | |
| **FMDV / 225-254** | RRFHFDIDVS | AKDGYKI-N- | S-K-LDIIKA | LEDT |
| **EMCV / 232-266** | RRITFDYSVS | AGPVCSKTEA | GYKVLDVERA | FRPTG |

85

**FIGURE 15. Characterization of PV 2C$^{ATPase}$ triple alanine mutants.** (a) Growth

properties of mutants at different temperatures. The location of N$_{252}$ and of the triple

alanine mutants on the 2C$^{ATPase}$ sequence is illustrated on top. RNA transcripts of wt and

mutant constructs were transfected into HeLa R19 monolayers and incubated at 33$^{o}$C,

37$^{o}$C, and 39.5$^{o}$C for 48 hours or until CPE (Materials and Methods). Freeze-thawed

supernatants were used to passage on fresh HeLa R19 monolayers. The genotypes of

recovered progeny viruses from 33$^{o}$C passages are indicated. (b, c) Virus titers and

plaque phenotypes of viable mutants: QVM/AVA and EYS/AAA. Viruses derived from

33$^{o}$C transfections were plaqued at 33$^{o}$C, 37$^{o}$C and 39.5$^{o}$C and the titers were determined

(Materials and Methods). The plaque phenotypes of the viruses at different temperatures

are shown at the indicated dilutions.

**(a)**
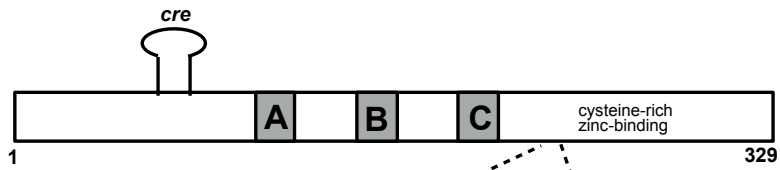


|  | | Growth Phenotype | | | Genotype of progeny (33°C) |
|---|---|:---:|:---:|:---:|:---:|
|  | | 33°C | 37°C | 39.5°C | |
| WT ⇒ | FDMDIQVMNEYSRDGKL | + | + | + | WT |
| FMI/AAA ⇒ | A–A–A–––––––––––––– | - | - | - | - |
| QVM /AAA ⇒ | –––––AAA–––––––––– | + | + | - | AVA |
| EYS/AAA ⇒ | –––––––––AAA–––––– | + | + | + | AAA |
| GKL/AAA ⇒ | –––––––––––––––AAA | - | - | - | - |

**(b)**
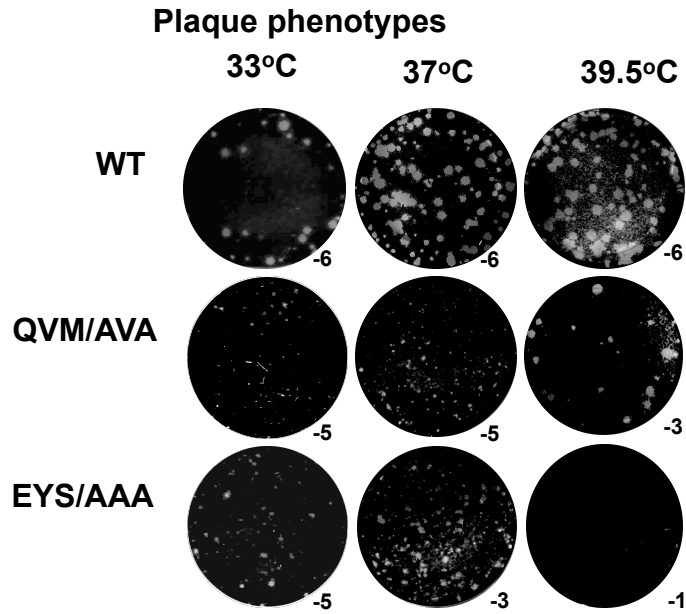


**(c)**

**Plaque phenotypes**
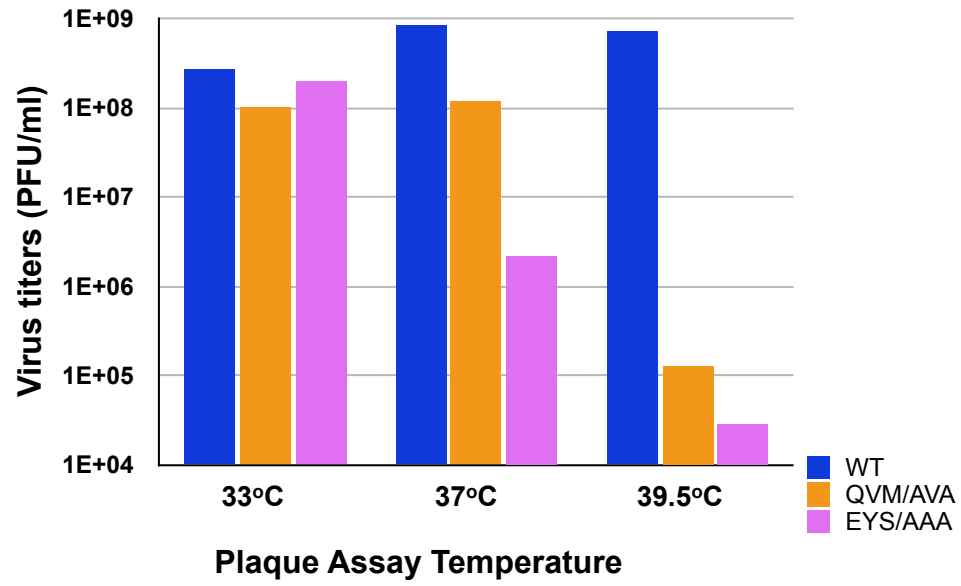
**FIGURE 16. Temperature sensitive triple alanine mutants are defective in RNA replication at 39$^o$C.** RNA levels in HeLa cells infected with viable mutants, EYS/AAA and variant QVM/AVA. HeLa cells were infected at an m.o.i. of 5 with wt and mutant viruses obtained from 33$^o$C transfections. The infected cells were harvested at various time points after infection and total RNA was isolated from the lysates. RNA levels were determined by qPCR, as described in Materials and Methods.
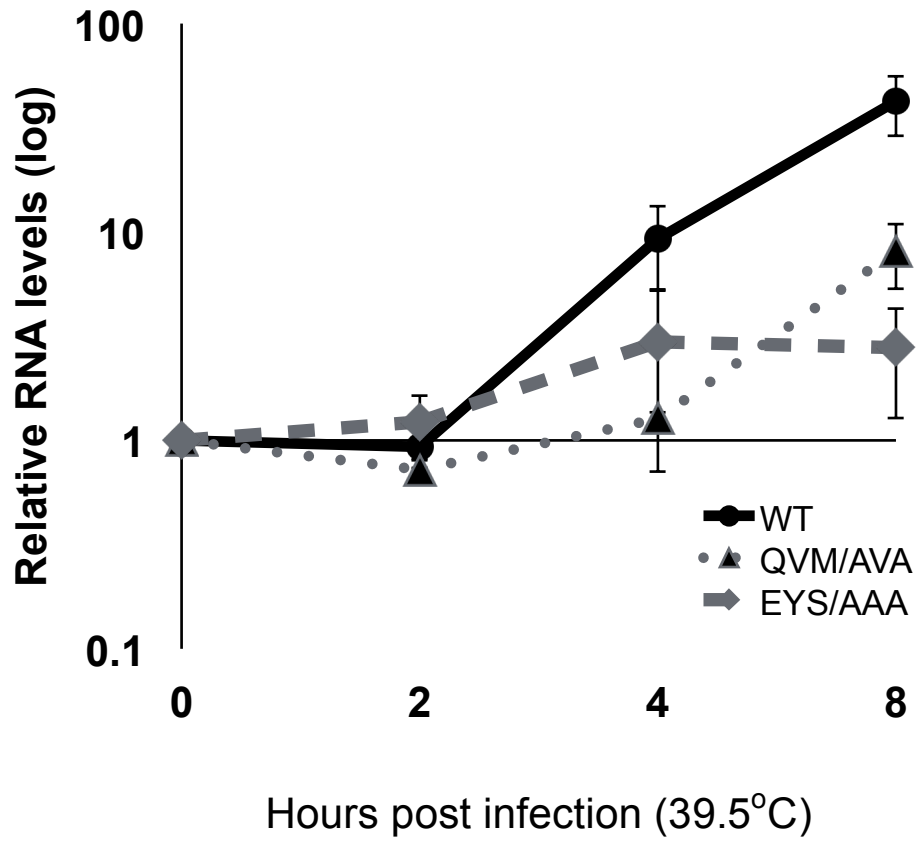
**FIGURE 17.** *In vitro* **translation of wt and non-viable mutant (FMI/AAA and GKL/AAA) transcript RNAs.** Transcript RNAs of the wt and of the lethal mutants were translated in HeLa cell-free extracts at $34^{o}$C for 8 hrs as described in (Materials and Methods). None of the mutants exhibited abnormal translation or processing.
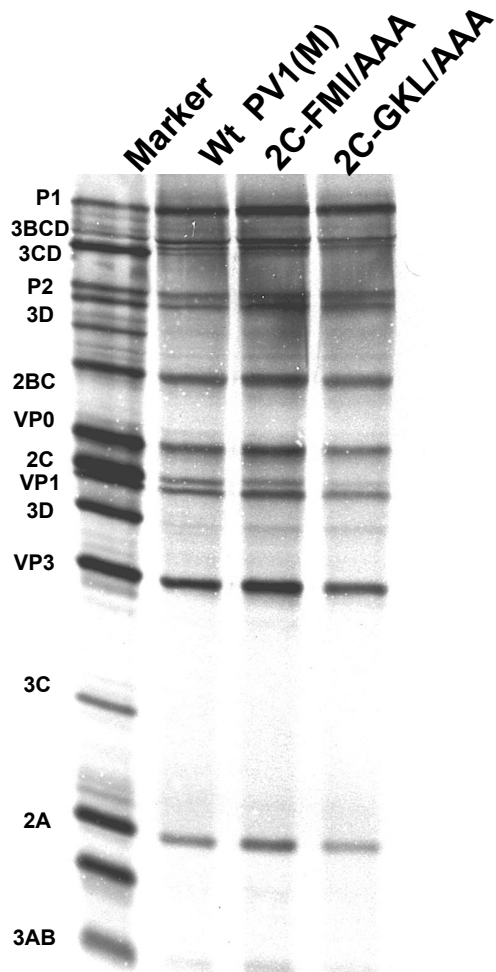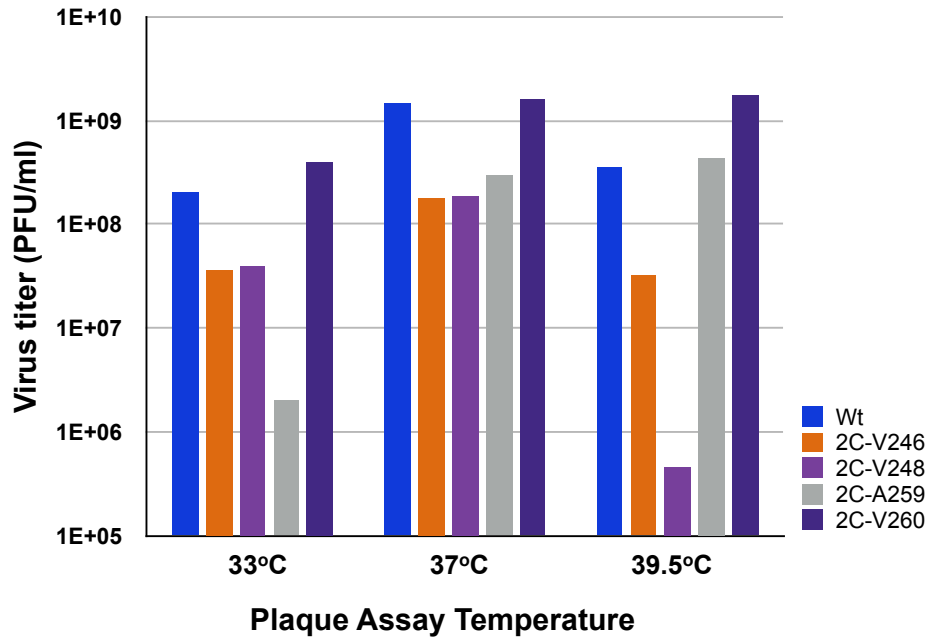
**FIGURE 18. Growth phenotypes of single alanine mutants.** (a) Virus viability and the genotype of progeny at 37$^{\circ}$C. Single alanine mutants, derived from the two nonviable triple amino acid mutants FMI/AAA and GKL/AAA, were generated. They were tested for viability at 37$^{\circ}$C and the genotypes of the progeny were determined. (b) Virus titers and plaque phenotypes of single alanine mutants. Viruses grown at 37$^{\circ}$C were titered at 33$^{\circ}$C, 37$^{\circ}$C and 39.5$^{\circ}$C by plaque assay (Materials and Methods). (c) The plaque phenotypes are shown on the right panel. Subscripts indicate the virus dilution at which the image was taken. It should be noted that the mixed plaque sizes seen with the M$_{246}$A lysate (39.5$^{\circ}$C) presumably contains a mixture of the original alanine mutant (small) and of the V variant (large).

**(a)**

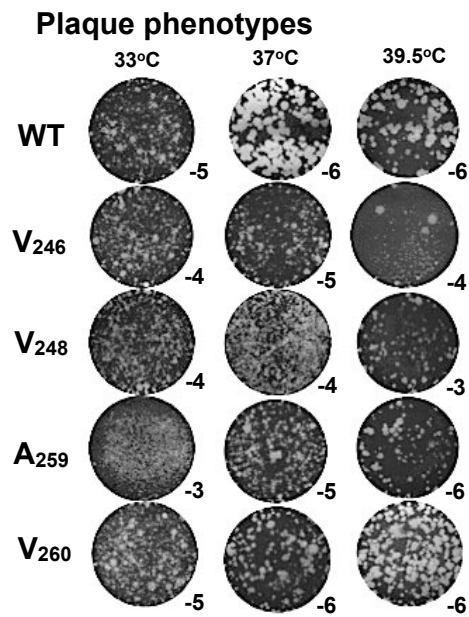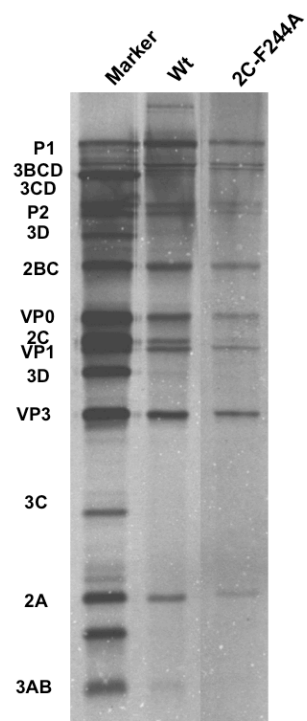| | | Virus Viability (37°C) | Genotype of progeny (37°C) |
|---|---|---|---|
| | 244                260 | | |
| WT ⇒ | FDMDIQVMNEYSRDGKL | + | WT |
| $F_{244}A$ ⇒ | A – – – – – – – – – – – – – – – – | - | - |
| $M_{246}A$ ⇒ | – – A – – – – – – – – – – – – – – | + | $A_{246}V$ |
| $I_{248}A$ ⇒ | – – – – A – – – – – – – – – – – – | + | $A_{248}V$ |
| $K_{259}A$ ⇒ | – – – – – – – – – – – – – – A – | + | $A_{259}$ |
| $L_{260}A$ ⇒ | – – – – – – – – – – – – – – – – A | + | $A_{260}V$ |

94

**(b)**



**(c)**

**FIGURE 19. The F$_{244}$A single mutation in PV 2C$^{ATPase}$ is lethal.** Non-viable single alanine mutation (F$_{244}$A) were used were further characterized. (a) In vitro translation of wt and F$_{244}$A RNA transcripts. Transcripts RNAs of wt and lethal mutant were translated in HeLa cell-free extracts for 8 hrs at 34$^{o}$C. (b) Nonviable mutant is defective in a RNA replication. Infected cells were harvested at various time points after transfection. Cells were washed twice, and the total RNAs were isolated from cell lysates. RNA levels were determined by qPCR as described in Material and Methods.
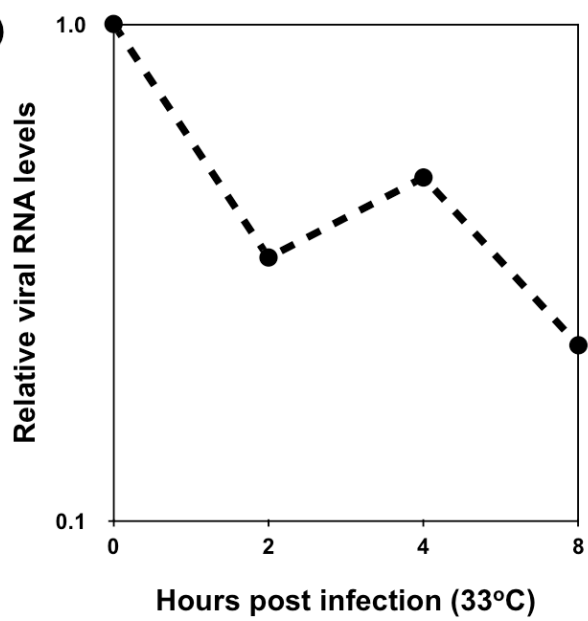
**(a)**

Marker | Wt | 2C-F244A

P1
3BCD
3CD
P2
3D
2BC
VP0
2C
VP1
3D
VP3
3C
2A
3AB

**(b)**

Relative viral RNA levels

Hours post infection (33°C)

**FIGURE 20. The 2C$^{ATPase}$ K$_{259}$A mutant is delayed in virus production and protein synthesis at the restrictive temperatures (35$^o$C and 33$^o$C).** (a) Growth curves of wt and K$_{259}$A mutant polioviruses at the permissive (37$^o$C) and restrictive (35$^o$C and 33$^o$C) temperatures. HeLa cells were infected at an m.o.i. of 5 with viruses derived from 37$^o$C transfections. The viral progeny was titered by plaque assay at different times post-infection by plaque assay (Materials and Methods). Black lines: growth curves at 37$^o$C; grey lines: growth curves at 33$^o$C. (b) Protein synthesis by the wt and K$_{259}$A mutant measured by Western analysis. HeLa cells were infected either at 33$^o$C, 35$^o$C or 37$^o$C at an m.o.i. of 5 with purified viruses derived from 37$^o$C infections. The infected cells were isolated at various times post-infection and lysed. The level of 2C$^{ATPase}$-related proteins and of capsid protein VP3 were measured by SDS-page/Western analysis using a monoclonal antibody to 2C$^{ATPase}$ and a polyclonal antibody to VP3, respectively, as described in Materials and Methods.
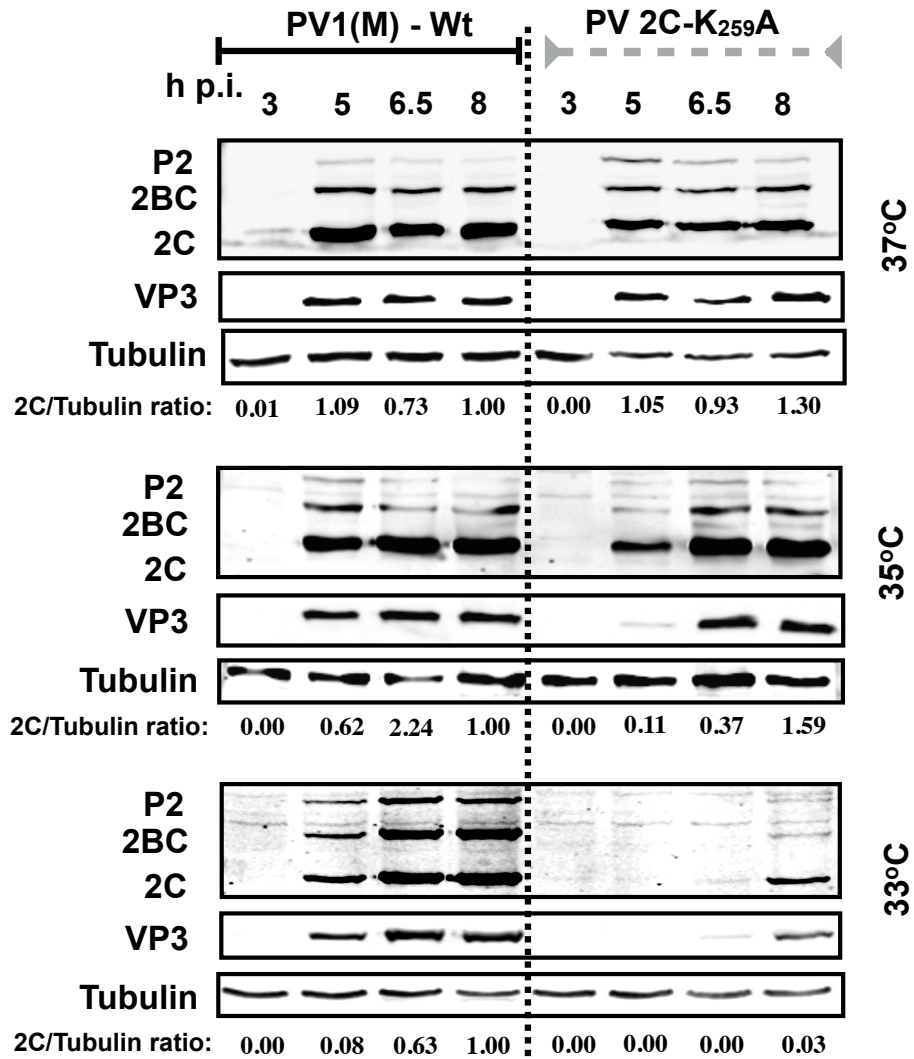
**(a)**
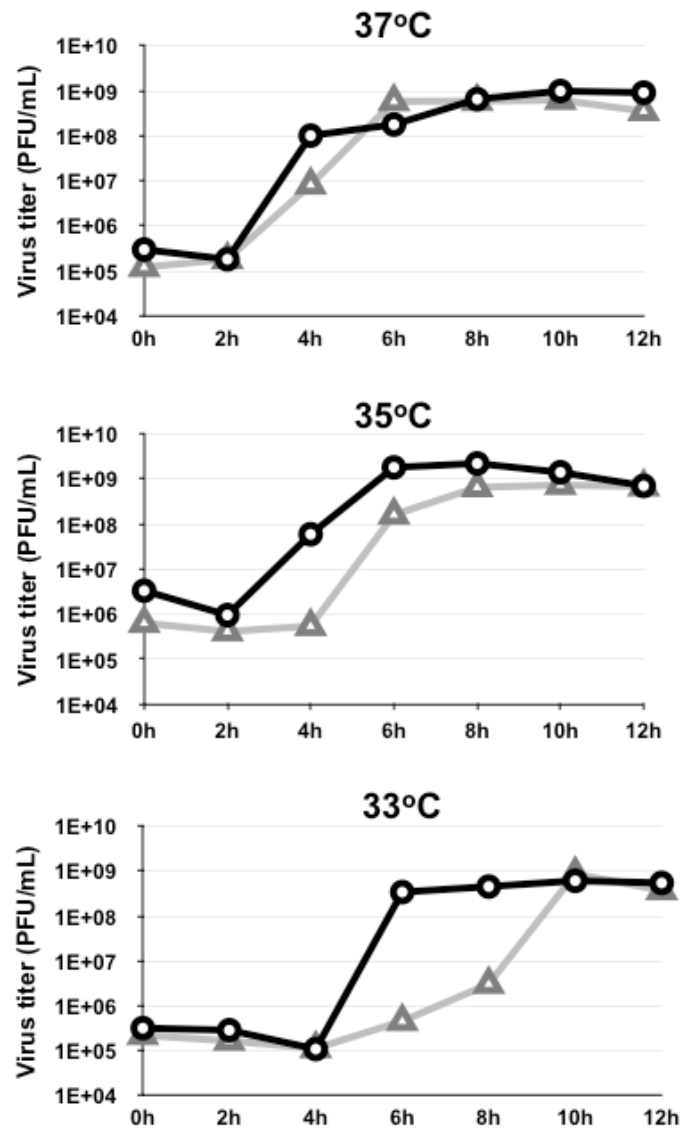
**(b)**

**FIGURE 21. The K$_{259}$A 2C$^{ATPase}$ mutant possesses an encapsidation defect at 33$^o$C.**

Genome structure of a Renilla luciferase (R-Luc) Reporter virus (R-Luc-PPP). The R-Luc

gene was fused between the 5'NTR and P1 structural proteins, flanked by a 3CD$^{pro}$

cleavage site. Wt and mutant K$_{259}$A 2C$^{ATPase}$ reporter virus RNA transcripts were

transfected into HeLa cells at 33$^o$C or 37$^o$C, both in the absence and presence of GnHCl

(Materials and Methods). R-Luc assays were performed at 8 hr post-transfection.

Aliquots of the lysates from the transfections were used to infect fresh HeLa cells, both in

the absence and presence of GnHCl. R-Luc assays were performed at 8 hr post infection.

R-Luc ratios were calculated by dividing the raw R-Luc values in the absence over the R-

Luc values in the presence of GnHCl.
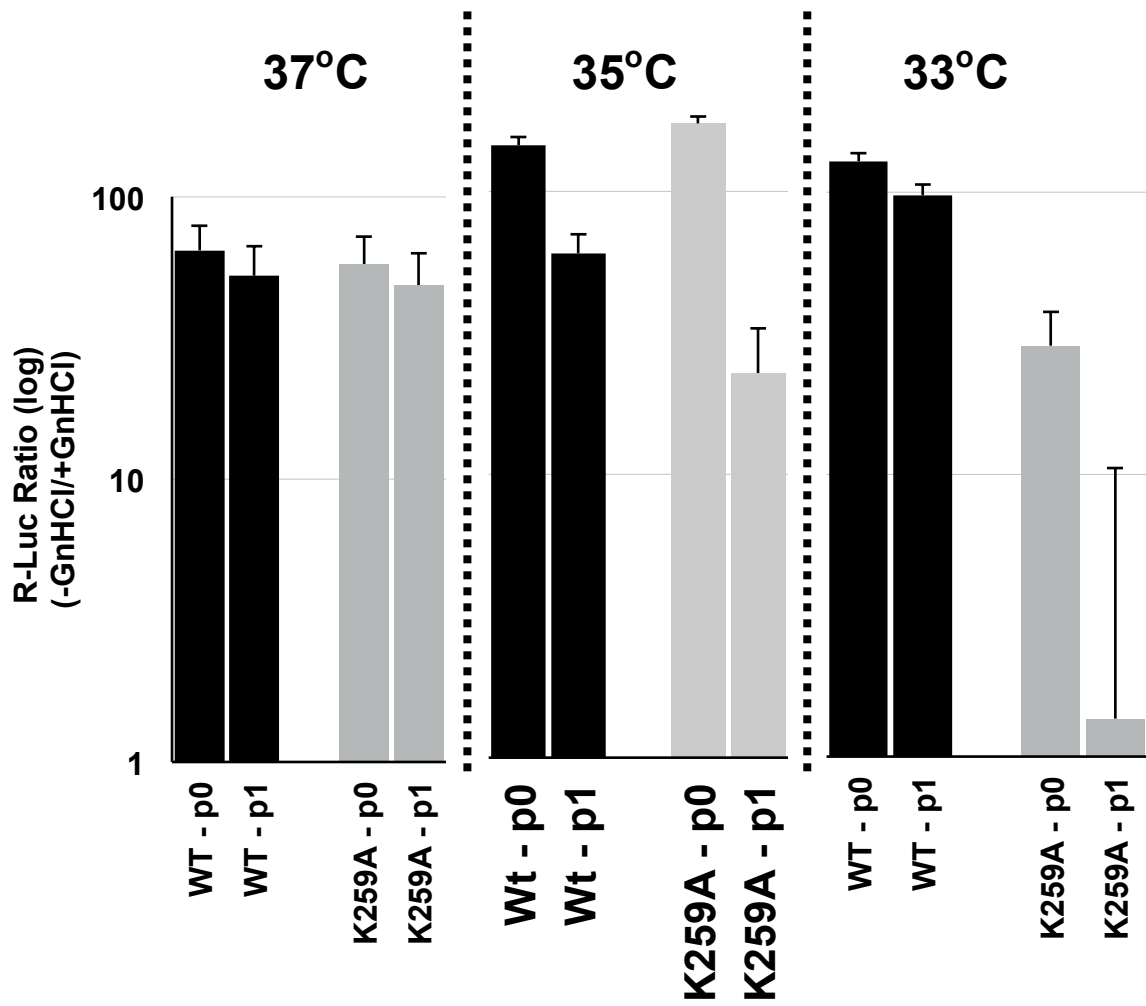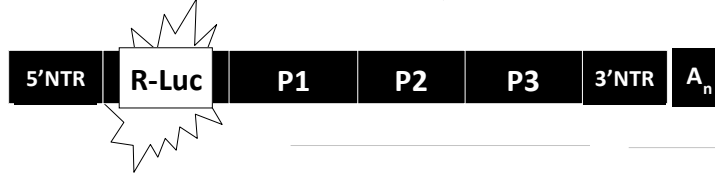
**FIGURE 22. Immunofluorescence imaging of and K$_{259}$A mutant virus-infected HeLa cells.** HeLa cells were infected with wt or 2C-K$_{259}$A virus at an m.o.i. of 5. Cells were incubated for 4 hr (37$^o$C), 5 hr (35$^o$C), or 6 hr (33$^o$C) and were fixed with paraformaldehyde. Infected cells were probed with primary antibody against 2C$^{ATPase}$ and mature virus (McAb A12), followed by alexa fluor 555 (red) and 488 (green) conjugated antibodies, respectively. The cell nucleus was stained with DAPI, shown in blue.

**Wt - PVM Infection**     **2C-K$_{259}$A PVM Infection**
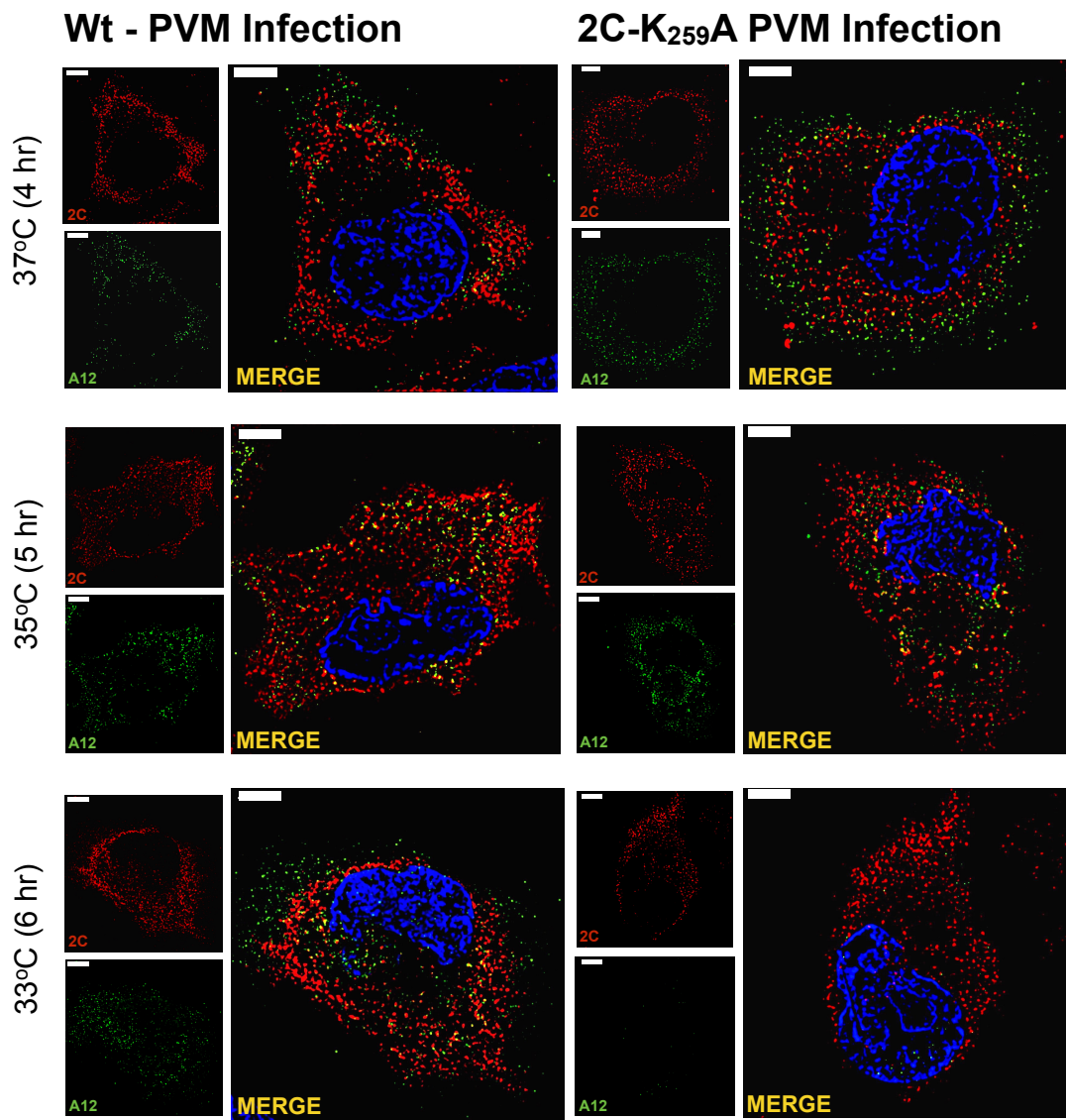
**Table 2**: Summary of the growth phenotypes of individual amino acid mutants of non-viable FMI/AAA and GKL/AAA mutants.

| Mutants | Wt (nt) | Alanine (nt) | Time of full CPE | Growth phenotype of alanine mutant | Variant | Growth phenotype of variant mutant |
|---------|---------|--------------|------------------|-------------------------------------|---------|-------------------------------------|
| $F_{244}A$ | TTC | gcC | - | non-viable | - | - |
| $M_{246}A$ | ATG | gcc | Tf | viable | gTc(valine) | *t.s.* |
| $I_{248}A$ | ATT | gcc | Tf | *q.i.* | gTc(valine) | *t.s.* |
| $K_{259}A$ | AAA | gcA | Tf | *c.s.* | gcA | *c.s.* |
| $L_{260}A$ | TTG | gca | P1 | *q.i.* | gTa(valine) | wt-like |

*t.s.* – temperature sensitive; *c.s.* – cold sensitive; *q.i.* – quasi infectious

# REFERENCES

Adams, P., Kandiah, E., Effantin, G., Steven, A.C., Ehrenfeld, E., 2009. Poliovirus 2C Protein Forms Homo-oligomeric Structures Required for ATPase Activity. J. Biol. Chem. 284, 22012–22021. doi:10.1074/jbc.M109.031807

Aldabe, R., Carrasco, L., 1995a. Induction of membrane proliferation by poliovirus proteins 2C and 2BC. Biochem. Biophys. Res. Commun. 206, 64–76. doi:10.1006/bbrc.1995.1010

Aldabe, R., Carrasco, L., 1995b. Induction of membrane proliferation by poliovirus proteins 2C and 2BC. Biochem. Biophys. Res. Commun. 206, 64–76. doi:10.1006/bbrc.1995.1010

Alexander, H.E., Koch, G., Mountain, I.M., Sprunt, K., van Damme, O., 1958. Infectivity of ribonucleic acid of poliovirus on HeLa cell mono-layers. Virology 5, 172–173.

Andino, R., Rieckhof, G.E., Baltimore, D., 1990. A functional ribonucleoprotein complex forms around the 5' end of poliovirus RNA. Cell 63, 369–380.

Arita, M., Wakita, T., Shimizu, H., 2012. Valosin-Containing Protein (VCP/p97) Is Required for Poliovirus Replication and Is Involved in Cellular Protein Secretion Pathway in Poliovirus Infection. Journal of Virology 86, 5541–5553. doi:10.1128/JVI.00114-12

Arita, M., Zhu, S.-L., Yoshida, H., Yoneyama, T., Miyamura, T., Shimizu, H., 2005. A Sabin 3-derived poliovirus recombinant contained a sequence homologous with indigenous human enterovirus species C in the viral polymerase coding region.

Journal of Virology 79, 12650–12657. doi:10.1128/JVI.79.20.12650-12657.2005

Baltimore, D., 1968. Structure of the poliovirus replicative intermediate RNA. Journal of Molecular Biology 32, 359–368.

Banerjee, R., Weidman, M.K., Echeverri, A., Kundu, P., Dasgupta, A., 2004. Regulation of poliovirus 3C protease by the 2C polypeptide. Journal of Virology 78, 9243–9256. doi:10.1128/JVI.78.17.9243-9256.2004

Barclay, W., Li, Q., Hutchinson, G., Moon, D., Richardson, A., Percy, N., Almond, J.W., Evans, D.J., 1998. Encapsidation studies of poliovirus subgenomic replicons. J. Gen. Virol. 79 ( Pt 7), 1725–1734.

Basavappa, R., Syed, R., Flore, O., Icenogle, J.P., Filman, D.J., Hogle, J.M., 1994. Role and mechanism of the maturation cleavage of VP0 in poliovirus assembly: structure of the empty capsid assembly intermediate at 2.9 A resolution. Protein Sci. 3, 1651–1669. doi:10.1002/pro.5560031005

Bedard, K.M., Semler, B.L., 2004. Regulation of picornavirus gene expression. Microbes Infect. 6, 702–713. doi:10.1016/j.micinf.2004.03.001

Belov, G.A., Altan-Bonnet, N., Kovtunovych, G., Jackson, C.L., Lippincott-Schwartz, J., Ehrenfeld, E., 2007. Hijacking components of the cellular secretory pathway for replication of poliovirus RNA. Journal of Virology 81, 558–567. doi:10.1128/JVI.01820-06

Berstein, H.D., Baltimore, D., 1988. Poliovirus mutant that contains a cold-sensitive defect in viral RNA synthesis. Journal of Virology 62, 2922–2928.

Bienz, K., Egger, D., Pasamontes, L., 1987. Association of polioviral proteins of the P2 genomic region with the viral replication complex and virus-induced membrane

synthesis as visualized by electron microscopic immunocytochemistry and autoradiography. Virology 160, 220–226.

Bienz, K., Egger, D., Pfister, T., 1994. Characteristics of the poliovirus replication complex. Arch. Virol. Suppl. 9, 147–157.

Bishop, J.M., Koch, G., 1967. Purification and characterization of poliovirus-induced infectious double-stranded ribonucleic acid. J. Biol. Chem. 242, 1736–1743.

Bishop, J.M., Koch, G., Evans, B., Merriman, M., 1969. Poliovirus replicative intermediate: structural basis of infectivity. Journal of Molecular Biology 46, 235–249.

Blyn, L.B., Swiderek, K.M., Richards, O., Stahl, D.C., Semler, B.L., Ehrenfeld, E., 1996. Poly(rC) binding protein 2 binds to stem-loop IV of the poliovirus RNA 5' noncoding region: identification by automated liquid chromatography-tandem mass spectrometry. Proc. Natl. Acad. Sci. U.S.A. 93, 11115–11120.

Borman, A.M., Kirchweger, R., Ziegler, E., Rhoads, R.E., Skern, T., Kean, K.M., 1997. elF4G and its proteolytic cleavage products: effect on initiation of protein synthesis from capped, uncapped, and IRES-containing mRNAs. RNA 3, 186–196.

Brandenburg, B., Lee, L.Y., Lakadamyali, M., Rust, M.J., Zhuang, X., Hogle, J.M., 2007. Imaging Poliovirus Entry in Live Cells. Plos Biol 5, e183. doi:10.1371/journal.pbio.0050183.sg002

Brunner, J.E., Ertel, K.J., Rozovics, J.M., Semler, B.L., 2010. Delayed kinetics of poliovirus RNA synthesis in a human cell line with reduced levels of hnRNP C proteins. Virology 400, 240–247. doi:10.1016/j.virol.2010.01.031

Brunner, J.E., Nguyen, J.H.C., Roehl, H.H., Ho, T.V., Swiderek, K.M., Semler, B.L., 2005.

Functional interaction of heterogeneous nuclear ribonucleoprotein C with poliovirus RNA synthesis initiation complexes. Journal of Virology 79, 3254–3266. doi:10.1128/JVI.79.6.3254-3266.2005

Burgon, T.B., Jenkins, J.A., Deitz, S.B., Spagnolo, J.F., Kirkegaard, K., 2009. Bypass Suppression of Small-Plaque Phenotypes by a Mutation in Poliovirus 2A That Enhances Apoptosis. Journal of Virology 83, 10129–10139. doi:10.1128/JVI.00642-09

Chen, Z., Fischer, E.R., Kouiavskaia, D., Hansen, B.T., Ludtke, S.J., Bidzhieva, B., Makiya, M., Agulto, L., Purcell, R.H., Chumakov, K., 2013. Cross-neutralizing human anti-poliovirus antibodies bind the recognition site for cellular receptor. Proc. Natl. Acad. Sci. U.S.A. 110, 20242–20247. doi:10.1073/pnas.1320041110

Cheng, Z., Yang, J., Xia, H., Qiu, Y., Wang, Z., Han, Y., Xia, X., Qin, C.F., Hu, Y., Zhou, X., 2013. The Nonstructural Protein 2C of a Picorna-Like Virus Displays Nucleic Acid Helix Destabilizing Activity That Can Be Functionally Separated from Its ATPase Activity. Journal of Virology 87, 5205–5218. doi:10.1128/JVI.00245-13

Cho, M.W., Teterina, N., Egger, D., Bienz, K., Ehrenfeld, E., 1994. Membrane rearrangement and vesicle induction by recombinant poliovirus 2C and 2BC in human cells. Virology 202, 129–145. doi:10.1006/viro.1994.1329

Chow, M., Moscufo, N., 1995. [37] Myristoyl modification of viral proteins: Assays to assess functional roles, in: Lipid Modifications of Proteins, Methods in Enzymology. Elsevier, pp. 495–509. doi:10.1016/0076-6879(95)50093-6

Cuconati, A., Xiang, W., Lahser, F., Pfister, T., Wimmer, E., 1998. A protein linkage map of the P2 nonstructural proteins of poliovirus. Journal of Virology 72, 1297–

1307.

Curry, S., Chow, M., Hogle, J.M., 1996. The poliovirus 135S particle is infectious. Journal of Virology 70, 7125–7131.

Darnell, J.E., 1958. Adsorption and maturation of poliovirus in singly and multiply infected HeLa cells. J. Exp. Med. 107, 633–641.

De Sena, J., Mandel, B., 1977. Studies on the in vitro uncoating of poliovirus. II. Characteristics of the membrane-modified particle. Virology 78, 554–566.

De Sena, J., Torian, B., 1980. Studies on the in vitro uncoating of poliovirus. III. Roles of membrane-modifying and -stabilizing factors in the generation of subviral particles. Virology 104, 149–163.

Detjen, B.M., Lucas, J., Wimmer, E., 1978. Poliovirus single-stranded RNA and double-stranded RNA: differential infectivity in enucleate cells. Journal of Virology 27, 582–586.

Diamond, S.E., Kirkegaard, K., 1994. Clustered charged-to-alanine mutagenesis of poliovirus RNA-dependent RNA polymerase yields multiple temperature-sensitive mutants defective in RNA synthesis. Journal of Virology 68, 863–876.

Doedens, J.R., Kirkegaard, K., 1995. Inhibition of cellular protein secretion by poliovirus proteins 2B and 3A. EMBO J. 14, 894–907.

Echeverri, A., Banerjee, R., Dasgupta, A., 1998. Amino-terminal region of poliovirus 2C protein is sufficient for membrane binding. Virus Res. 54, 217–223.

Ender, J.F., Weller, T.H., Robbins, F.C., 1949. Cultivation of the Lansing strain of poliomyelitis virus in cultures of various human embryonic tissues. Science.

Fenwick, M.L., Wall, M.J., 1973. Factors determining the site of synthesis of

poliovirus proteins: the early attachment of virus particles to endoplasmic membranes. J. Cell. Sci. 13, 403–413.

Finch, J.T., Klug, A., 1959. Structure of poliomyelitis virus. Nature 183, 1709–1714.

Flanegan, J.B., Baltimore, D., 1977. Poliovirus-specific primer-dependent RNA polymerase able to copy poly(A). Proc. Natl. Acad. Sci. U.S.A. 74, 3677–3680.

Gamarnik, A.V., Andino, R., 1998. Switch from translation to RNA replication in a positive-stranded RNA virus. Genes Dev. 12, 2293–2304.

Gamarnik, A.V., Andino, R., 2000. Interactions of viral protein 3CD and poly(rC) binding protein with the 5' untranslated region of the poliovirus genome. Journal of Virology 74, 2219–2226.

Geller, R., Vignuzzi, M., Andino, R., Frydman, J., 2007. Evolutionary constraints on chaperone-mediated folding provide an antiviral approach refractory to development of drug resistance. Genes Dev. 21, 195–205. doi:10.1101/gad.1505307

Gmyl, A.P., Pilipenko, E.V., Maslova, S.V., Belov, G.A., Agol, V.I., 1993. Functional and genetic plasticities of the poliovirus genome: quasi-infectious RNAs modified in the 5'-untranslated region yield a variety of pseudorevertants. Journal of Virology 67, 6309–6316.

Goodfellow, I., Chaudhry, Y., Richardson, A., Meredith, J., Almond, J.W., Barclay, W., Evans, D.J., 2000. Identification of a cis-acting replication element within the poliovirus coding region. Journal of Virology 74, 4590–4600.

Gorbalenya, A.E., Koonin, E.V., 1993. Helicases: amino acid sequence comparisons and structure-function relationships. Current opinion in structural biology 3,

419–429. doi:10.1002/pro.5560070309

Gromeier, M., Alexander, L., Wimmer, E., 1996. Internal ribosomal entry site substitution eliminates neurovirulence in intergeneric poliovirus recombinants. Proc. Natl. Acad. Sci. U.S.A. 93, 2370–2375.

Guillot, S., Otelea, D., Delpeyroux, F., Crainic, R., 1994. Point mutations involved in the attenuation/neurovirulence alternation in type 1 and 2 oral polio vaccine strains detected by site-specific polymerase chain reaction. Vaccine 12, 503–507.

Guttman, N., Baltimore, D., 1977. Morphogenesis of poliovirus. IV. existence of particles sedimenting at 150S and having the properties of provirion. Journal of Virology 23, 363–367.

Hanecak, R., Semler, B.L., Anderson, C.W., Wimmer, E., 1982. Proteolytic processing of poliovirus polypeptides: antibodies to polypeptide P3-7c inhibit cleavage at glutamine-glycine pairs. Proc. Natl. Acad. Sci. U.S.A. 79, 3973–3977.

Harber, J.J., Bradley, J., Anderson, C.W., Wimmer, E., 1991. Catalysis of poliovirus VP0 maturation cleavage is not mediated by serine 10 of VP2. Journal of Virology 65, 326–334.

Harris, K.S., Xiang, W., Alexander, L., Lane, W.S., Paul, A.V., Wimmer, E., 1994. Interaction of poliovirus polypeptide 3CDpro with the 5" and 3" termini of the poliovirus genome. Identification of viral and cellular cofactors needed for efficient binding. J. Biol. Chem. 269, 27004–27014.

Hellen, C.U., Kräusslich, H.G., Wimmer, E., 1989. Proteolytic processing of polyproteins in the replication of RNA viruses. Biochemistry 28, 9881–9890.

Hellen, C.U., Wimmer, E., 1992. Maturation of poliovirus capsid proteins. Virology 187, 391–397.

Herold, J., Andino, R., 2001. Poliovirus RNA replication requires genome circularization through a protein-protein bridge. Mol. Cell 7, 581–591.

Hindiyeh, M., Li, Q.H., Basavappa, R., Hogle, J.M., Chow, M., 1999. Poliovirus mutants at histidine 195 of VP2 do not cleave VP0 into VP2 and VP4. Journal of Virology 73, 9072–9079.

Hogle, J.M., 2002. Poliovirus cell entry: common structural themes in viral cell entry pathways. Annu. Rev. Microbiol. 56, 677–702. doi:10.1146/annurev.micro.56.012302.160757

Horne, R.W., Nagington, J., 1959. Electron microscope studies of the development and structure of poliomyelitis virus. Journal of Molecular Biology 1, 333–IN8. doi:10.1016/S0022-2836(59)80015-2

Hsu, N.-Y., Ilnytska, O., Belov, G., Santiana, M., Chen, Y.-H., Takvorian, P.M., Pau, C., van der Schaar, H., Kaushik-Basu, N., Balla, T., Cameron, C.E., Ehrenfeld, E., van Kuppeveld, F.J.M., Altan-Bonnet, N., 2010. Viral reorganization of the secretory pathway generates distinct organelles for RNA replication. Cell 141, 799–811. doi:10.1016/j.cell.2010.03.050

Jang, S.K., Kräusslich, H.G., Nicklin, M.J., Duke, G.M., Palmenberg, A.C., Wimmer, E., 1988. A segment of the 5' nontranslated region of encephalomyocarditis virus RNA directs internal entry of ribosomes during in vitro translation. Journal of Virology 62, 2636–2643.

Jiang, P., Faase, J.A.J., Toyoda, H., Paul, A., Wimmer, E., Gorbalenya, A.E., 2007.

Evidence for emergence of diverse polioviruses from C-cluster coxsackie A viruses and implications for global poliovirus eradication. Proc. Natl. Acad. Sci. U.S.A. 104, 9457–9462. doi:10.1073/pnas.0700451104

Jiang, P., Liu, Y., Ma, H.C., Paul, A.V., Wimmer, E., 2014. Picornavirus Morphogenesis. Microbiology and Molecular Biology Reviews 78, 418–437. doi:10.1128/MMBR.00012-14

Jordan, L., Mayor, H.D., 1974. Studies on the degradation of poliovirus by heat. Microbios 9, 51–60.

Katagiri, S., Hinuma, Y., Ishida, N., 1967. Biophysical properties of poliovirus particles irradiated with ultraviolet light. Virology 32, 337–343. doi:10.1016/0042-6822(67)90282-6

Kelley, L.A., Sternberg, M.J.E., 2009. Protein structure prediction on the Web: a case study using the Phyre server. Nat Protoc 4, 363–371. doi:10.1038/nprot.2009.2

Kew, O., Morris-Glasgow, V., Landaverde, M., Burns, C., Shaw, J., Garib, Z., André, J., Blackman, E., Freeman, C.J., Jorba, J., Sutter, R., Tambini, G., Venczel, L., Pedreira, C., Laender, F., Shimizu, H., Yoneyama, T., Miyamura, T., van Der Avoort, H., Oberste, M.S., Kilpatrick, D., Cochi, S., Pallansch, M., de Quadros, C., 2002. Outbreak of poliomyelitis in Hispaniola associated with circulating type 1 vaccine-derived poliovirus. Science 296, 356–359. doi:10.1126/science.1068284

Kew, O.M., Sutter, R.W., de Gourville, E.M., Dowdle, W.R., Pallansch, M.A., 2005. Vaccine-derived polioviruses and the endgame strategy for global polio eradication. Annu. Rev. Microbiol. 59, 587–635.

doi:10.1146/annurev.micro.58.030603.123625

Kitamura, N., Semler, B.L., Rothberg, P.G., Larsen, G.R., Adler, C.J., Dorner, A.J., Emini, E.A., Hanecak, R., Lee, J.J., van der Werf, S., Anderson, C.W., Wimmer, E., 1981a. Primary structure, gene organization and polypeptide expression of poliovirus RNA. Nature 291, 547–553.

Kitamura, N., Semler, B.L., Rothberg, P.G., Larsen, G.R., Adler, C.J., Dorner, A.J., Emini, E.A., Hanecak, R., Lee, J.J., van der Werf, S., Anderson, C.W., Wimmer, E., 1981b. Primary structure, gene organization and polypeptide expression of poliovirus RNA. , Published online: 18 June 1981; | doi:10.1038/291547a0 291, 547–553. doi:10.1038/291547a0

Koch, F., Koch, G., 1985. The Molecular Biology of Poliovirus. Springer.

Kohn, A., 1979. Early interactions of viruses with cellular membranes. Adv. Virus Res. 24, 223–276.

Korant, B.D., 1973. Cleavage of poliovirus-specific polypeptide aggregates. Journal of Virology 12, 556–563.

Kräusslich, H.G., Nicklin, M.J., Toyoda, H., Etchison, D., Wimmer, E., 1987. Poliovirus proteinase 2A induces cleavage of eucaryotic initiation factor 4F polypeptide p220. Journal of Virology 61, 2711–2718.

Kuhn, R.J., Wimmer, E., 1987. replication of picornaviruses. Molecular biology of the positive strand RNA viruses / editors, D.J. Rowlands, M.A. Mayo, B.W.J. Mahy.

Lawson, M.A., Semler, B.L., 1992. Alternate poliovirus nonstructural protein processing cascades generated by primary sites of 3C proteinase cleavage. Virology 191, 309–320.

Lenarcic, E.M., Landry, D.M., Greco, T.M., Cristea, I.M., Thompson, S.R., 2013.
Thiouracil cross-linking mass spectrometry: a cell-based method to identify host
factors involved in viral amplification. Journal of Virology 87, 8697–8712.
doi:10.1128/JVI.00950-13

Levy, H.B., 1961. Intracellular sites of poliovirus reproduction. Virology 15, 173–
184.

Li, J.-P., Baltimore, D., 1990. An intragenic revertant of a poliovirus 2C mutant has an
uncoating defect. Journal of Virology 64, 1102–1107.

Li, J.P., Baltimore, D., 1988. Isolation of poliovirus 2C mutants defective in viral RNA
synthesis. Journal of Virology.

Liu, Y., Wang, C., Mueller, S., Paul, A.V., Wimmer, E., Jiang, P., 2010. Direct Interaction
between Two Viral Proteins, the Nonstructural Protein 2CATPase and the
Capsid Protein VP3, Is Required for Enterovirus Morphogenesis. PLoS Pathog 6,
e1001066. doi:10.1371/journal.ppat.1001066.s001

Lonberg-Holm, K., Gosser, L.B., Kauer, J.C., 1975. Early alteration of poliovirus in
infected cells and its specific inhibition. J gen Virol.

Ma, H.-C., Liu, Y., Wang, C., Strauss, M., Rehage, N., Chen, Y.-H., Altan-Bonnet, N.,
Hogle, J., Wimmer, E., Mueller, S., Paul, A.V., Jiang, P., 2014. An Interaction
between Glutathione and the Capsid Is Required for the Morphogenesis of C-
Cluster Enteroviruses. PLoS Pathog 10, e1004052.
doi:10.1371/journal.ppat.1004052.t001

Macadam, A.J., Ferguson, G., Arnold, C., Minor, P.D., 1991. An assembly defect as a
result of an attenuating mutation in the capsid proteins of the poliovirus type 3

vaccine strain. Journal of Virology 65, 5225–5231.

Maizel, J.V., Phillips, B.A., Summers, D.F., 1967. Composition of artificially produced and naturally occurring empty capsids of poliovirus type 1. Virology 32, 692–699.

Melnick, J.L., 1996. Current status of poliovirus infections. Clinical Microbiology Reviews 9, 293–300.

Minor, P., 2009. Vaccine-derived poliovirus (VDPV): Impact on poliomyelitis eradication. Vaccine 27, 2649–2652. doi:10.1016/j.vaccine.2009.02.071

Mirzayan, C., Wimmer, E., 1994. Biochemical studies on poliovirus polypeptide 2C: evidence for ATPase activity. Virology 199, 176–187. doi:10.1006/viro.1994.1110

Molla, A., Paul, A.V., Wimmer, E., 1991. Cell-free, de novo synthesis of poliovirus. Science 254, 1647–1651.

Nomoto, A., Kitamura, N., Golini, F., Wimmer, E., 1977. The 5'-terminal structures of poliovirion RNA and poliovirus mRNA differ only in the genome-linked protein VPg. Proc. Natl. Acad. Sci. U.S.A. 74, 5345–5349.

Nomoto, A., Lee, Y.F., Wimmer, E., 1976. The 5' end of poliovirus mRNA is not capped with m7G(5')ppp(5')Np. Proc. Natl. Acad. Sci. U.S.A. 73, 375–380.

Nugent, C.I., Kirkegaard, K., 1995. RNA binding properties of poliovirus subviral particles. Journal of Virology 69, 13–22.

Pallansch, M.A., Sandhu, H.S., 2006. The eradication of polio--progress and challenges. N. Engl. J. Med. 355, 2508–2511. doi:10.1056/NEJMp068200

Paul, A.V., Cao, X., Harris, K.S., Lama, J., Wimmer, E., 1994a. Studies with poliovirus

polymerase 3Dpol. Stimulation of poly(U) synthesis in vitro by purified

poliovirus protein 3AB. J. Biol. Chem. 269, 29173–29181.

Paul, A.V., Molla, A., Wimmer, E., 1994b. Studies of a putative amphipathic helix in

the N-terminus of poliovirus protein 2C. Virology 199, 188–199.

doi:10.1006/viro.1994.1111

Paul, A.V., Peters, J., Mugavero, J., Yin, J., van Boom, J.H., Wimmer, E., 2003.

Biochemical and genetic studies of the VPg uridylylation reaction catalyzed by

the RNA polymerase of poliovirus. Journal of Virology 77, 891–904.

doi:10.1128/JVI.77.2.891-904.2003

Paul, A.V., Rieder, E., Kim, D.W., van Boom, J.H., Wimmer, E., 2000. Identification of

an RNA hairpin in poliovirus RNA that serves as the primary template in the in

vitro uridylylation of VPg. Journal of Virology 74, 10359–10370.

Paul, A.V., Schultz, A., Pincus, S.E., Oroszlan, S., Wimmer, E., 1987. Capsid protein VP4

of poliovirus is N-myristoylated. Proc. Natl. Acad. Sci. U.S.A. 84, 7827–7831.

Paul, A.V., Wimmer, E., 2015. Initiation of protein-primed picornavirus RNA

synthesis. Virus Res. 1–15. doi:10.1016/j.virusres.2014.12.028

Pelletier, J., Kaplan, G., Racaniello, V.R., Sonenberg, N., 1988. Translational efficiency

of poliovirus mRNA: mapping inhibitory cis-acting elements within the 5'

noncoding region. Journal of Virology 62, 2219–2227.

Perera, R., Daijogo, S., Walter, B.L., Nguyen, J.H.C., Semler, B.L., 2007. Cellular protein

modification by poliovirus: the two faces of poly(rC)-binding protein. Journal of

Virology 81, 8919–8932. doi:10.1128/JVI.01013-07

Pfister, T., Egger, D., Bienz, K., 1995. Poliovirus subviral particles associated with

progeny RNA in the replication complex. J. Gen. Virol. 76 ( Pt 1), 63–71.

Pfister, T., Jones, K.W., Wimmer, E., 2000. A Cysteine-Rich Motif in Poliovirus Protein 2CATPase Is Involved in RNA Replication and Binds Zinc In Vitro. Journal of Virology 74, 334–343. doi:10.1128/JVI.74.1.334-343.2000

Pfister, T., Wimmer, E., 1999. Characterization of the nucleoside triphosphatase activity of poliovirus protein 2C reveals a mechanism by which guanidine inhibits poliovirus replication. J. Biol. Chem. 274, 6992–7001.

Phillips, B.A., Fennell, R., 1973. Polypeptide composition of poliovirions, naturally occurring empty capsids, and 14S precursor particles. Journal of Virology 12, 291–299.

Pincus, S.E., Diamond, D.C., Emini, E.A., Wimmer, E., 1986. Guanidine-selected mutants of poliovirus: mapping of point mutations to polypeptide 2C. Journal of Virology 57, 638–646.

Racaniello, V.R., Baltimore, D., 1981. Cloned poliovirus complementary DNA is infectious in mammalian cells. Science 214, 916–919. doi:10.1126/science.6272391

Richards, A.L., Soares-Martins, J.A.P., Riddell, G.T., Jackson, W.T., 2014. Generation of unique poliovirus RNA replication organelles. MBio 5, e00833–13. doi:10.1128/mBio.00833-13

Rieder, E., Paul, A.V., Kim, D.W., van Boom, J.H., Wimmer, E., 2000. Genetic and biochemical studies of poliovirus cis-acting replication element cre in relation to VPg uridylylation. Journal of Virology 74, 10371–10380.

Rieder, E., Xiang, W., Paul, A., Wimmer, E., 2003. Analysis of the cloverleaf element in

a human rhinovirus type 14/poliovirus chimera: correlation of subdomain D structure, ternary protein complex formation and virus replication. J. Gen. Virol. 84, 2203–2216.

Rivera, V.M., Welsh, J.D., Maizel, J.V., 1988. Comparative sequence analysis of the 5' noncoding region of the enteroviruses and rhinoviruses. Virology 165, 42–50.

Rodríguez, P.L., Carrasco, L., 1993. Poliovirus protein 2C has ATPase and GTPase activities. J. Biol. Chem. 268, 8105–8110.

Rodríguez, P.L., Carrasco, L., 1995. Poliovirus protein 2C contains two regions involved in RNA binding activity. J. Biol. Chem. 270, 10105–10112.

Roehl, H.H., Semler, B.L., 1995. Poliovirus infection enhances the formation of two ribonucleoprotein complexes at the 3' end of viral negative-strand RNA. Journal of Virology 69, 2954–2961.

Rombaut, B., Vrijsen, R., Boeyé, A., 1983. Epitope evolution in poliovirus maturation. Arch. Virol. 76, 289–298.

Rombaut, B., Vrijsen, R., Boeyé, A., 1990. New evidence for the precursor role of 14 S subunits in poliovirus morphogenesis. Virology 177, 411–414.

Rothberg, P.G., Harris, T.J., Nomoto, A., Wimmer, E., 1978. O4-(5'-uridylyl)tyrosine is the bond between the genome-linked protein and the RNA of poliovirus. Proc. Natl. Acad. Sci. U.S.A. 75, 4868–4872.

Rousset, D., Rakoto-Andrianarivelo, M., Razafindratsimandresy, R., Randriamanalina, B., Guillot, S., Balanant, J., Mauclère, P., Delpeyroux, F., 2003. Recombinant vaccine-derived poliovirus in Madagascar. Emerging Infect. Dis. 9, 885–887. doi:10.3201/eid0907.020692

Sabin, A.B., Boulger, L.R., 1973. History of Sabin attenuated poliovirus oral live

    vaccine strains. Journal of Biological Standardization 1, 115–118.

    doi:10.1016/0092-1157(73)90048-6

Salk, J.E., 1960. Persistence of immunity after administration of formalin-treated

    poliovirus vaccine. Lancet 2, 715–723.

Salk, J.E., Bennett, B.L., Lewis, L.J., Bazeley, P.L., 1954. Formaldehyde treatment and

    safety testing of experimental poliomyelitis vaccines. American Journal ….

    doi:10.1016/j.taap.2015.03.018

Schlegel, A., Giddings, T.H., Ladinsky, M.S., Kirkegaard, K., 1996. Cellular origin and

    ultrastructure of membranes induced during poliovirus infection. Journal of

    Virology 70, 6576–6588.

Shimizu, H., Thorley, B., Paladin, F.J., Brussen, K.A., Stambos, V., Yuen, L., Utama, A.,

    Tano, Y., Arita, M., Yoshida, H., Yoneyama, T., Benegas, A., Roesel, S., Pallansch,

    M., Kew, O., Miyamura, T., 2004. Circulation of type 1 vaccine-derived poliovirus

    in the Philippines in 2001. Journal of Virology 78, 13512–13521.

    doi:10.1128/JVI.78.24.13512-13521.2004

Smyth, M.S., Martin, J.H., 2002. Picornavirus uncoating. MP, Mol. Pathol. 55, 214–

    219.

Song, Y., Liu, Y., Ward, C.B., Mueller, S., Futcher, B., Skiena, S., Paul, A.V., Wimmer, E.,

    2012. Identification of two functionally redundant RNA elements in the coding

    sequence of poliovirus using computer-generated design. Proceedings of the

    National Academy of Sciences 109, 14301–14307.

    doi:10.1073/pnas.1211484109

Spector, D.H., Baltimore, D., 1974. Requirement of 3'-terminal poly(adenylic acid) for the infectivity of poliovirus RNA. Proc. Natl. Acad. Sci. U.S.A. 71, 2983–2987.

Springer, C.L., Huntoon, H.P., Peersen, O.B., 2013. Polyprotein Context Regulates the Activity of Poliovirus 2CATPase Bound to Bilayer Nanodiscs. Journal of Virology 87, 5994–6004. doi:10.1128/JVI.03491-12

Stanway, G., Hughes, P.J., Mountford, R.C., Reeve, P., Minor, P.D., Schild, G.C., Almond, J.W., 1984. Comparison of the complete nucleotide sequences of the genomes of the neurovirulent poliovirus P3/Leon/37 and its attenuated Sabin vaccine derivative P3/Leon 12a1b. Proc. Natl. Acad. Sci. U.S.A. 81, 1539–1543.

Suhy, D.A., Giddings, T.H., Kirkegaard, K., 2000. Remodeling the endoplasmic reticulum by poliovirus infection and by individual viral proteins: an autophagy-like origin for virus-induced vesicles. Journal of Virology 74, 8953–8965.

Summers, D.F., Maizel, J.V., 1968. Evidence for large precursor proteins in poliovirus synthesis. Proc. Natl. Acad. Sci. U.S.A. 59, 966–971.

Sweeney, T.R., Cisnetto, V., Bose, D., Bailey, M., Wilson, J.R., Zhang, X., Belsham, G.J., Curry, S., 2010. Foot-and-Mouth Disease Virus 2C Is a Hexameric AAA+ Protein with a Coordinated ATP Hydrolysis Mechanism. J. Biol. Chem. 285, 24347–24359. doi:10.1074/jbc.M110.129940

Tang, W.F., Yang, S.Y., Wu, B.W., Jheng, J.R., Chen, Y.L., Shih, C.H., Lin, K.H., Lai, H.C., Tang, P., Horng, J.T., 2007. Reticulon 3 Binds the 2C Protein of Enterovirus 71 and Is Required for Viral Replication. Journal of Biological Chemistry 282, 5888–5898. doi:10.1074/jbc.M611145200

Teterina, N.L., Egger, D., Bienz, K., Brown, D.M., Semler, B.L., Ehrenfeld, E., 2001.

Requirements for assembly of poliovirus replication complexes and negative-strand RNA synthesis. Journal of Virology 75, 3841–3850. doi:10.1128/JVI.75.8.3841-3850.2001

Teterina, N.L., Gorbalenya, A.E., Egger, D., Bienz, K., Ehrenfeld, E., 1997. Poliovirus 2C protein determinants of membrane binding and rearrangements in mammalian cells. Journal of Virology 71, 8962–8972.

Teterina, N.L., Lauber, C., Jensen, K.S., Levenson, E.A., Gorbalenya, A.E., Ehrenfeld, E., 2011. Identification of tolerated insertion sites in poliovirus non-structural proteins. Virology 409, 1–11. doi:10.1016/j.virol.2010.09.028

Teterina, N.L., Levenson, E., Rinaudo, M.S., Egger, D., Bienz, K., Gorbalenya, A.E., Ehrenfeld, E., 2006. Evidence for functional protein interactions required for poliovirus RNA replication. Journal of Virology 80, 5327–5337. doi:10.1128/JVI.02684-05

Toyoda, H., Franco, D., Fujita, K., Paul, A.V., Wimmer, E., 2007. Replication of poliovirus requires binding of the poly(rC) binding protein to the cloverleaf as well as to the adjacent C-rich spacer sequence between the cloverleaf and the internal ribosomal entry site. Journal of Virology 81, 10017–10028. doi:10.1128/JVI.00516-07

Toyoda, H., Nicklin, M.J., Murray, M.G., Anderson, C.W., Dunn, J.J., Studier, F.W., Wimmer, E., 1986. A second virus-encoded proteinase involved in proteolytic processing of poliovirus polyprotein. Cell 45, 761–770.

Toyoda, H., Yang, C.F., Takeda, N., Nomoto, A., Wimmer, E., 1987. Analysis of RNA synthesis of type 1 poliovirus by using an in vitro molecular genetic approach.

Journal of Virology 61, 2816–2822.

Vance, L.M., Moscufo, N., Chow, M., Heinz, B.A., 1997. Poliovirus 2C region functions during encapsidation of viral RNA. Journal of Virology 71, 8759–8765.

Verlinden, Y., Cuconati, A., Wimmer, E., Rombaut, B., 2000. Cell-free synthesis of poliovirus: 14S subunits are the key intermediates in the encapsidation of poliovirus RNA. J. Gen. Virol. 81, 2751–2754.

Wang, C., Jiang, P., Sand, C., Paul, A.V., Wimmer, E., 2012. Alanine Scanning of Poliovirus 2CATPase Reveals New Genetic Evidence that Capsid Protein/2CATPase Interactions Are Essential for Morphogenesis. Journal of Virology 86, 9964–9975. doi:10.1128/JVI.00914-12

Wang, C., Ma, H.C., Wimmer, E., Jiang, P., Paul, A.V., 2014. A C-terminal, cysteine-rich site in poliovirus 2CATPase is required for morphogenesis. Journal of General Virology 95, 1255–1265. doi:10.1099/vir.0.062497-0

Wimmer, E., Hellen, C.U., Cao, X., 1993. Genetics of poliovirus. Annu. Rev. Genet. 27, 353–436. doi:10.1146/annurev.ge.27.120193.002033

Yin, J., Liu, Y., Wimmer, E., Paul, A.V., 2007. Complete protein linkage map between the P2 and P3 non-structural proteins of poliovirus. Journal of General Virology 88, 2259–2267. doi:10.1099/vir.0.82795-0

Yin, J., Paul, A.V., Wimmer, E., Rieder, E., 2003. Functional dissection of a poliovirus cis-acting replication element [PV-cre(2C)]: analysis of single- and dual-cre viral genomes and proteins that bind specifically to PV-cre RNA. Journal of Virology 77, 5152–5166. doi:10.1128/JVI.77.9.5152-5166.2003

Ypma-Wong, M.F., Filman, D.J., Hogle, J.M., Semler, B.L., 1988. Structural domains of

the poliovirus polyprotein are major determinants for proteolytic cleavage at Gln-Gly pairs. J. Biol. Chem. 263, 17846–17856.

Yu, X., Egelman, E.H., 1997. The RecA hexamer is a structural homologue of ring helicases. Nat. Struct. Biol. 4, 101–104.

Zell, R., Ihle, Y., Seitz, S., Gündel, U., Wutzler, P., Görlach, M., 2008. Poly(rC)-binding protein 2 interacts with the oligo(rC) tract of coxsackievirus B3. Biochem. Biophys. Res. Commun. 366, 917–921. doi:10.1016/j.bbrc.2007.12.038

Zhang, P., Mueller, S., Morais, M.C., Bator, C.M., Bowman, V.D., Hafenstein, S., Wimmer, E., Rossmann, M.G., 2008. Crystal structure of CD155 and electron microscopic studies of its complexes with polioviruses. Proceedings of the National Academy of Sciences 105, 18284–18289. doi:10.1073/pnas.0807848105